# Open Rotor Computational Aeroacoustic Analysis with an Immersed Boundary Method

Michael F. Barad§, Christoph Brehm*, Cetin C. Kiris§

Presented at

Stanford University

§Computational Aerosciences Branch
NASA Ames Research Center
*University of Arizona, Tucson

**May 4, 2016**

# Outline

1. Introduction to Acoustic Analysis of Contra Rotating Open Rotor
2. Numerical Methods
3. Computational and Experimental Setups
4. Comparison with Experiments
5. Brief Analysis Acoustic Near-Field for High and Low Speed Cases
6. Summary

# Introduction – The Big Picture

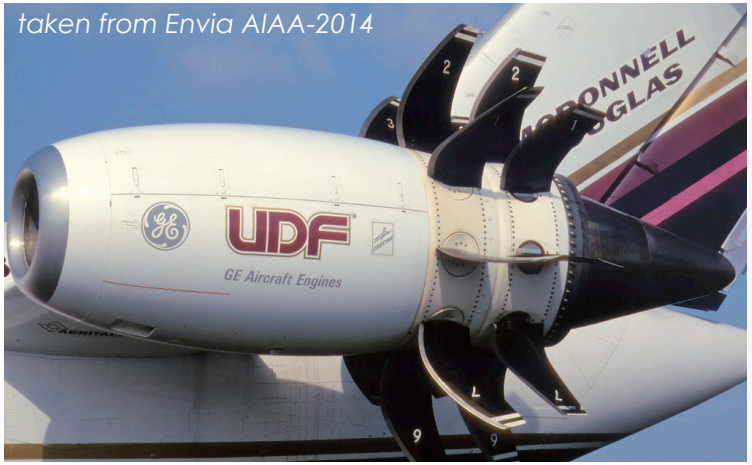


*GE36-UDF propfan demonstrator engine installed on MD-81 test bed aircraft (8x8)*

*Modern contra-rotating open rotor engine design from CFM (12x10)*

- Renewed interest in contra-rotating open rotor (CROR) propulsion technology due to large potential of significantly reducing fuel consumption
  (in context of HWB see Thomas et al. AIAA 2014-0258, Hendricks et al. AIAA 2013-3628)
- Noise generation from CROR is key concern and must meet community noise and cabin noise standards
- Reliable noise prediction capabilities are required for the design of low noise CROR systems

# Introduction – Previous Work


- NASA initiated several efforts that successfully addressed the noise prediction aspects for CROR mainly in free air

- There are two extreme approaches for modeling CROR noise
  a) Empirical models (cheap but lacks generality)
  b) Fully resolved CFD (general but too expensive)

- Model source region separate (hydrodynamics) from acoustic propagation

- Various tools are already available
  Acoustic: ASSPIN/ASSPIN2, FW-$H_{pds}$, FSC, LINPROP, QUADPROP
  Aerodynamics: SBAC, UBAC, FUN3D, Overflow, LAVA

- Different aspects of CROR noise generation have been studied

  - Tonal noise is the dominant part in the spectrum
    (Envia IJA-2015, Envia CMFF12-2012, VanZante and Envia ASME-2014, Nasr et al. AIAA 2013-3800, Sharma & Chen AIAA 2012-2265, Bush et al. AIAA 2013-2202)
  - Broadband noise can be important (flow conditions & observer angles)
    (Node-Langlois et al. AIAA 2014-2610, Sree & Stephens AIAA 2014-2744)
  - Initial attempts have been made to study installation effects
    (Dunn & Tinetti AIAA-2012-2217, Node-Langlois et al. AIAA 2014-2610)

# Introduction – Our Motivation

- A key challenge is to devise an efficient method that can capture installation effects
- Current approach:
  - Utilizing Cartesian AMR solver module within Launch Ascent and Vehicle Aerodynamics (LAVA) framework
  - Ffowcs-Williams and Hawkings (FW-H) method for acoustic noise propagation
  - Comparison with experiments and Housman & Kiris (2016) utilizing LAVA's curvilinear-overset solver
- **Objectives of this work:**

State-of-the-art in terms of efficiency & accuracy

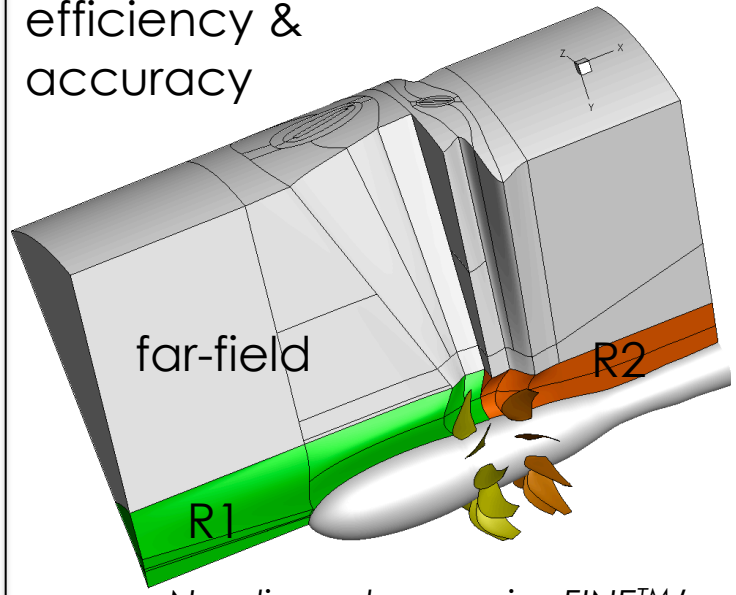


*Non-linear harmonics FINE™/ Turbo simulations and acoustic model for propagation*

Envia IJA-2015, Envia CMFF12-2012, VanZante & Envia ASME-2014

1. Develop moving boundary capabilities inside LAVA-Cartesian
2. Validate LAVA-Cartesian+FW-H approach against experimental data
3. Analyze noise propagation for nominal takeoff and cruise conditions

# Outline


1. Introduction to Acoustic Analysis of Contra Rotating Open Rotor
2. Numerical Methods
3. Computational and Experimental Setups
4. Comparison with Experiments
5. Brief Analysis Acoustic Near-Field for High and Low Speed Cases
6. Summary

# Launch Ascent & Vehicle Aerodynamics (LAVA)

LAVA is being developed at NASA Ames Research Center

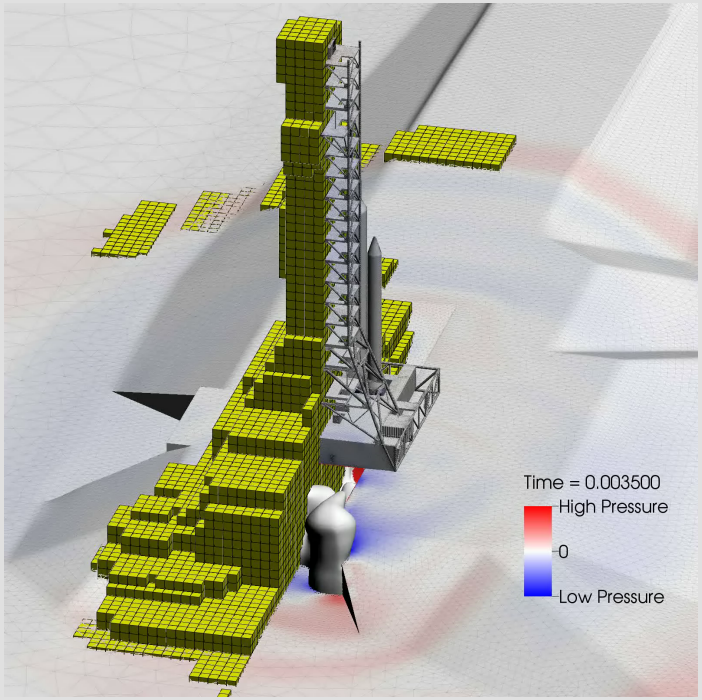


***Cartesian AMR***

- Essentially no manual grid generation
- Highly efficient Adaptive Mesh Refinement (AMR)
- Low computational cost
- Reliable higher order methods are available
- Non-body fitted -> Resolution of boundary layers problematic/ inefficient

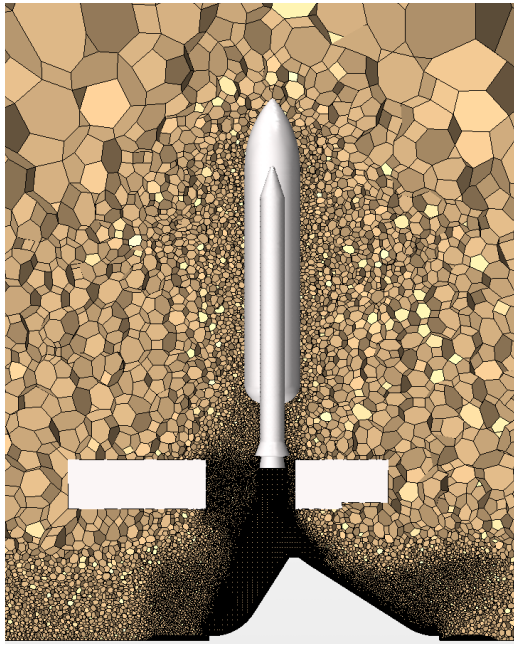

***Unstructured Arbitrary Polyhedral***

- Grid generation is mostly automated
- Body fitted grids
- Grid quality can be questionable
- High computational cost
- Higher order methods are yet to fully mature

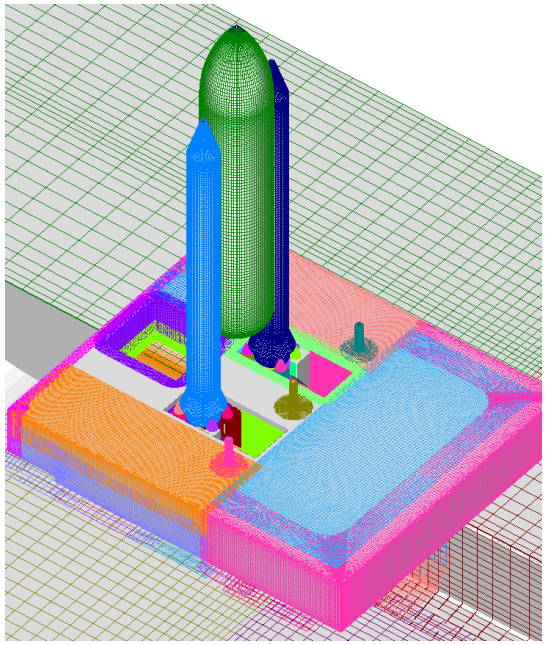

***Overset Structured Curvilinear***

- High quality, body fitted grids
- Low computational cost
- Reliable higher order methods are available
- Grid generation is largely manual and time consuming

*Kiris et al.(2014), Sozer et al. (2014), Brehm et al. (2014)

# Introduction – The Immersed Boundary Method

- Immersed boundary method (IB) allows automatic volume mesh generation from water tight surface triangulation
- For problems involving moving and deforming boundaries IB provides clear advantages (for example no mesh deformation needed)
- Main disadvantage is that at high Reynolds numbers, IBs become inefficient or require some type of wall function
- Most immersed boundary methods are only lower order accurate

Sharp higher-order IB inside LAVA-Cartesian:

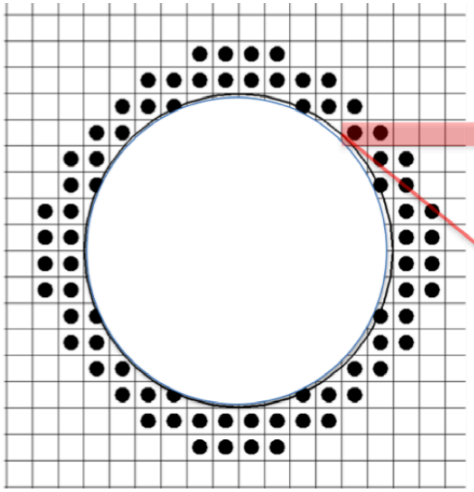

Circle immersed in Cartesian Grid

$$\mathbf{W}_t = \frac{\partial \mathbf{F}^+}{\partial \mathbf{W}} \cdot \frac{\partial \mathbf{W}}{\partial x} + \frac{\partial \mathbf{F}^-}{\partial \mathbf{W}} \cdot \frac{\partial \mathbf{W}}{\partial x}$$
$$\cong \frac{\partial \mathbf{F}^+}{\partial \mathbf{W}} \cdot (\underline{\mathbf{D}}_x^+ \cdot \mathbf{W}) + \frac{\partial \mathbf{F}^-}{\partial \mathbf{W}} \cdot (\underline{\mathbf{D}}_x^- \cdot \mathbf{W})$$

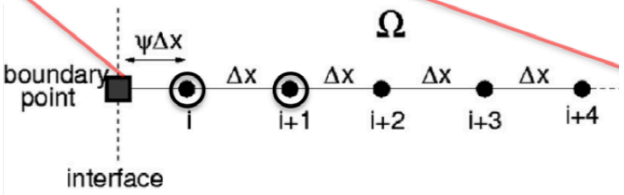


Setup in Vicinity of Immersed Boundary

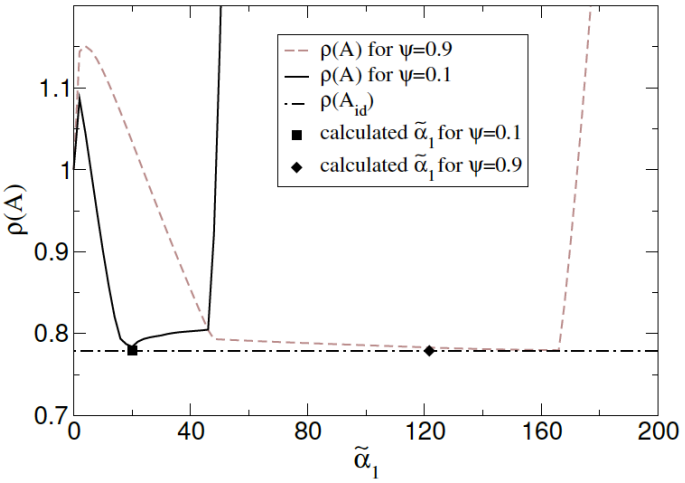


Dependence of Spectral Radius on free stencil coefficient

*Brehm et al. (JCP 2013, JCP 2015)*

# Introduction – The Immersed Boundary Method

- Imm… from…
- For p… adv…
- Mai… requ…
- Most immersed boundary methods are only lower order accurate

Extensions of original IB:

① Address IB challenges that are associated with the moving boundary problem.

② Deal with geometry queries and recomputation of irregular stencils in an efficient way.

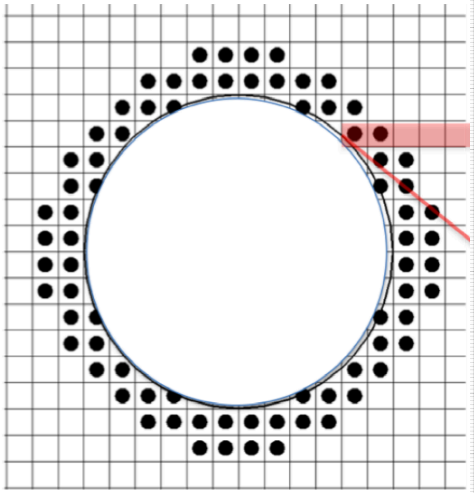

Circle immersed in Cartesian Grid

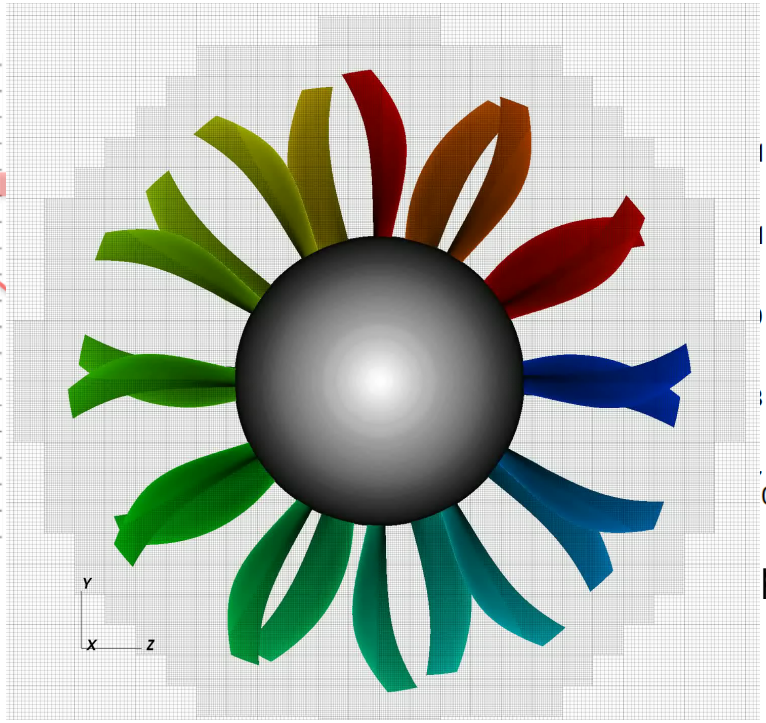


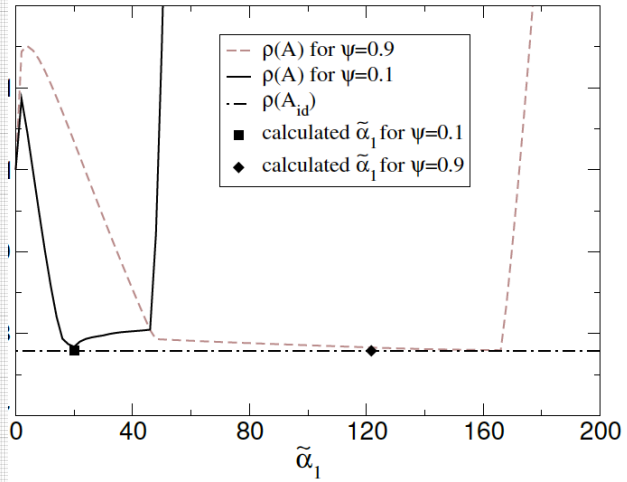


pendence of Spectral Radius on free stencil coefficient

*Brehm et al. (JCP 2013, JCP 2015)*

# IB Challenges for Moving Boundary Problems

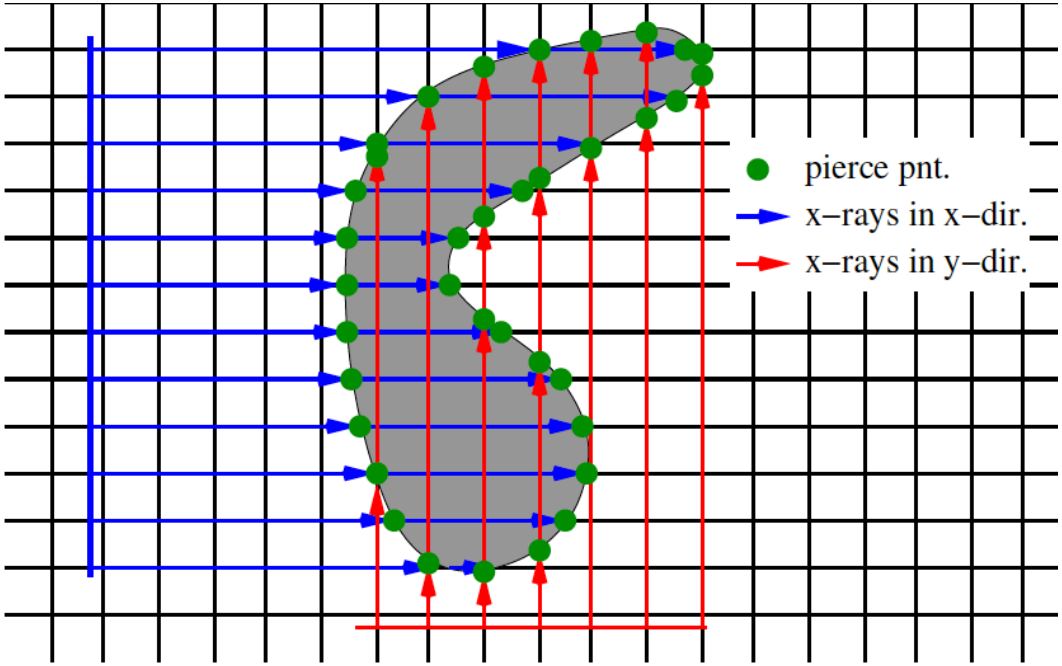


X-Ray Tracing Algorithm:

- Use discrete triangulations instead of level-set functions
- Using an optimized bounding volume hierarchy (BVH) based ray-tracing method [thanks to Intel's Embree and Tim Sandstrom]

# IB Challenges for Moving Boundary Problems

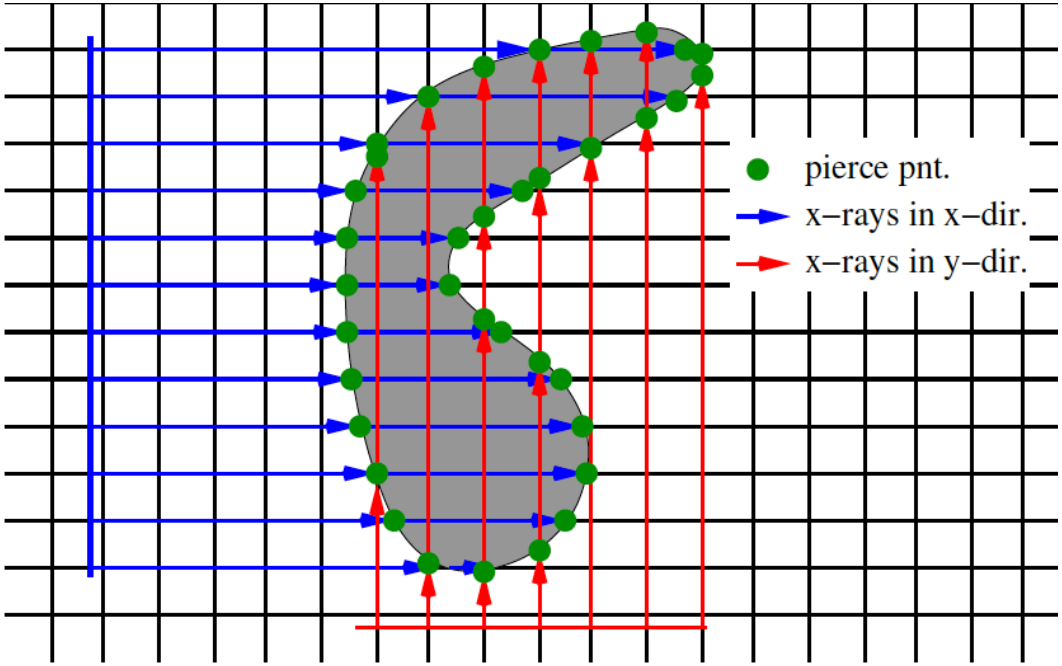


X-Ray Tracing Algorithm:

- Use discrete triangulations instead of level-set functions
- Using an optimized bounding volume hierarchy (BVH) based ray-tracing method [thanks to Intel's Embree and Tim Sandstrom]

Identification of Trapped Points:

- Occur in gaps that are smaller than irregular stencil size
- Current treatment is to reduce order of accuracy in the relevant direction

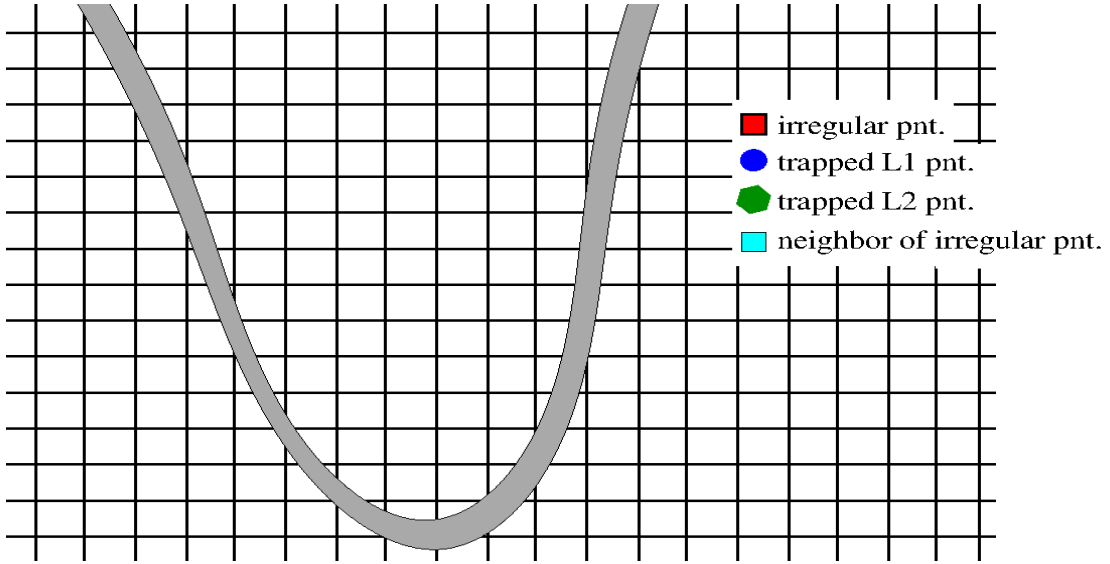

# IB Challenges for Moving Boundary Problems

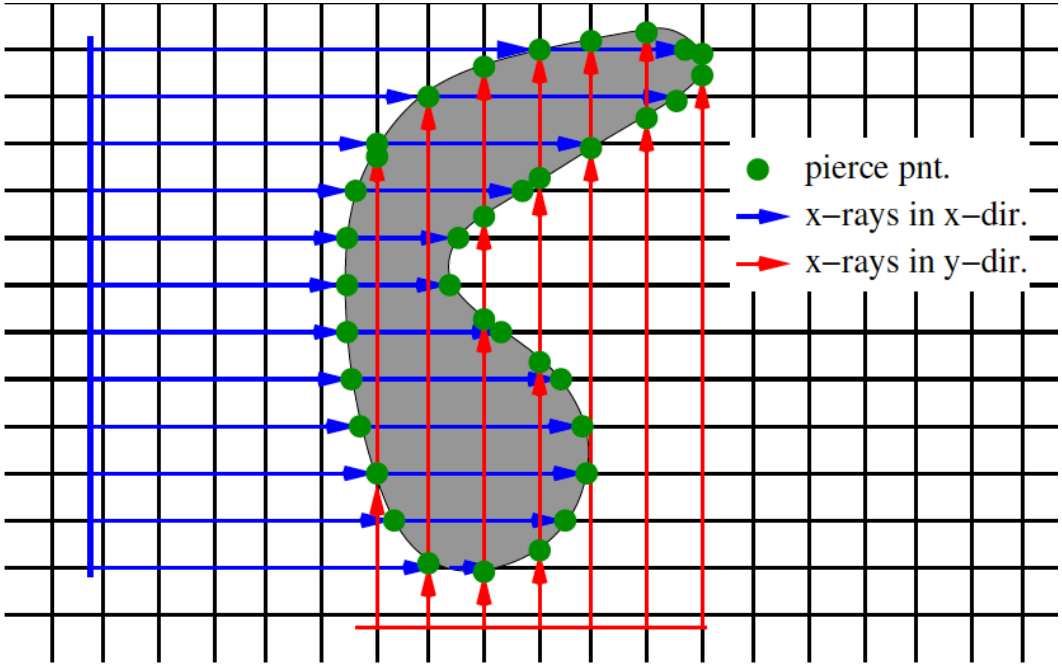


X-Ray Tracing Algorithm:

- Use discrete triangulations instead of level-set functions
- Using an optimized bounding volume hierarchy (BVH) based ray-tracing method [thanks to Intel's Embree and Tim Sandstrom]

Identification of Trapped Points:

- Occur in gaps that are smaller than irregular stencil size
- Current treatment is to reduce order of accuracy in the relevant direction

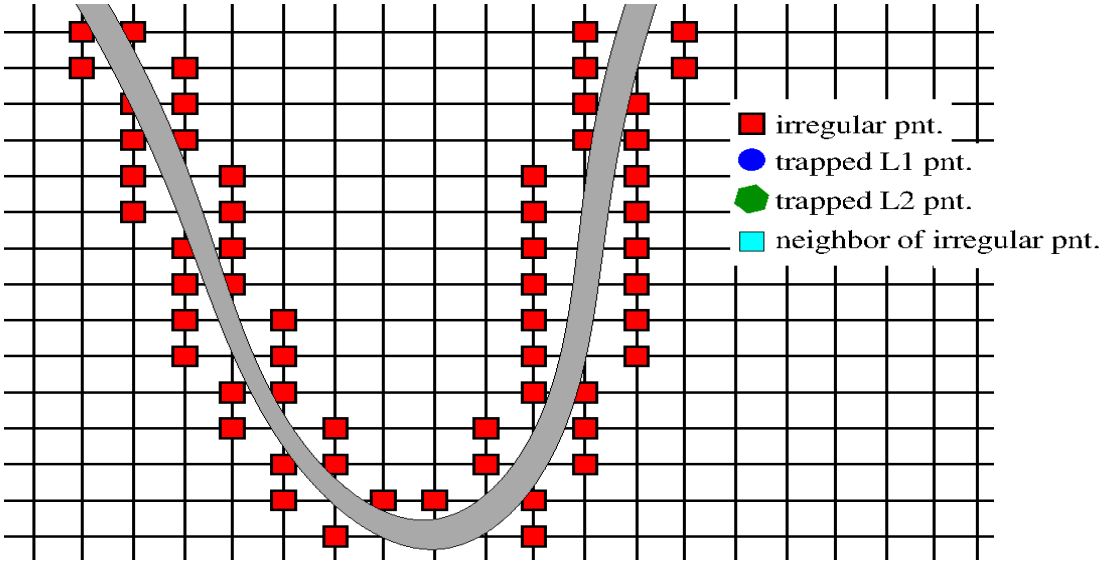

# IB Challenges for Moving Boundary Problems

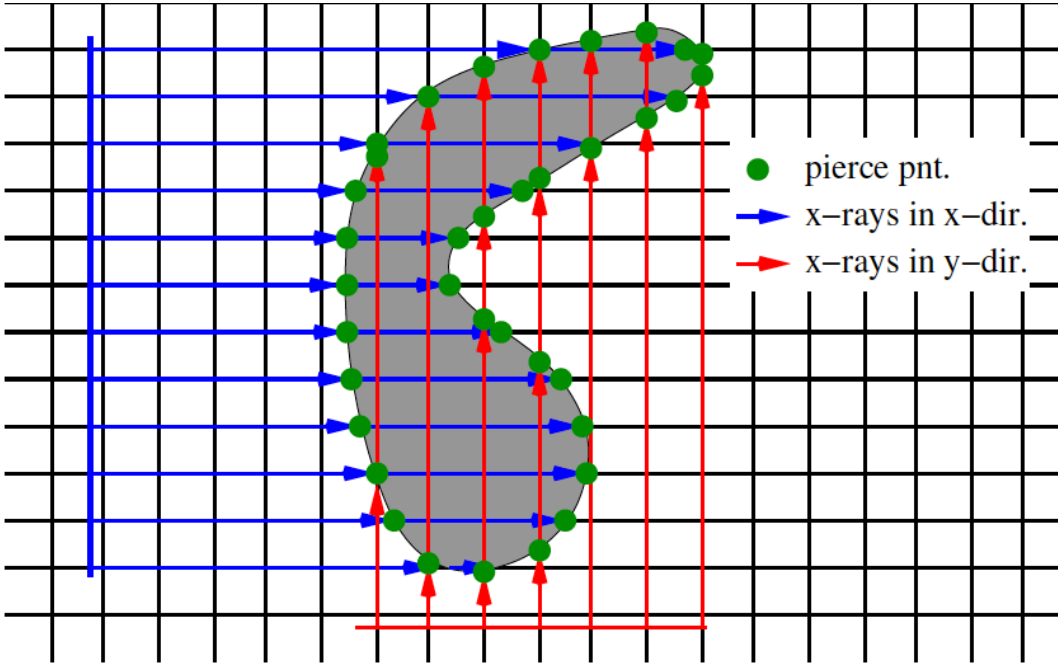


X-Ray Tracing Algorithm:

- Use discrete triangulations instead of level-set functions
- Using an optimized bounding volume hierarchy (BVH) based ray-tracing method [thanks to Intel's Embree and Tim Sandstrom]

Identification of Trapped Points:

- Occur in gaps that are smaller than irregular stencil size
- Current treatment is to reduce order of accuracy in the relevant direction

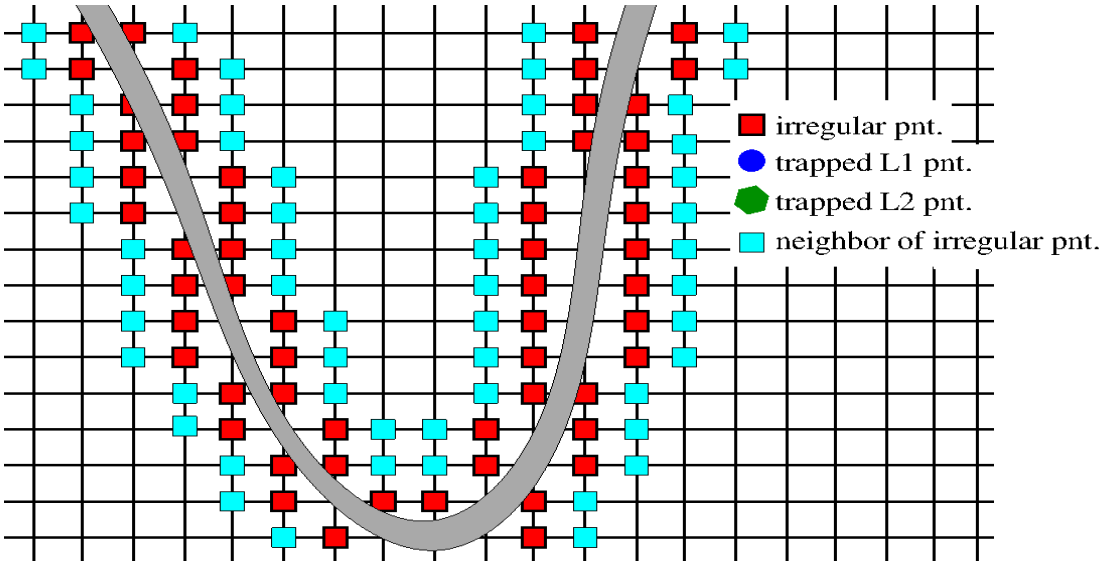

# IB Challenges for Moving Boundary Problems

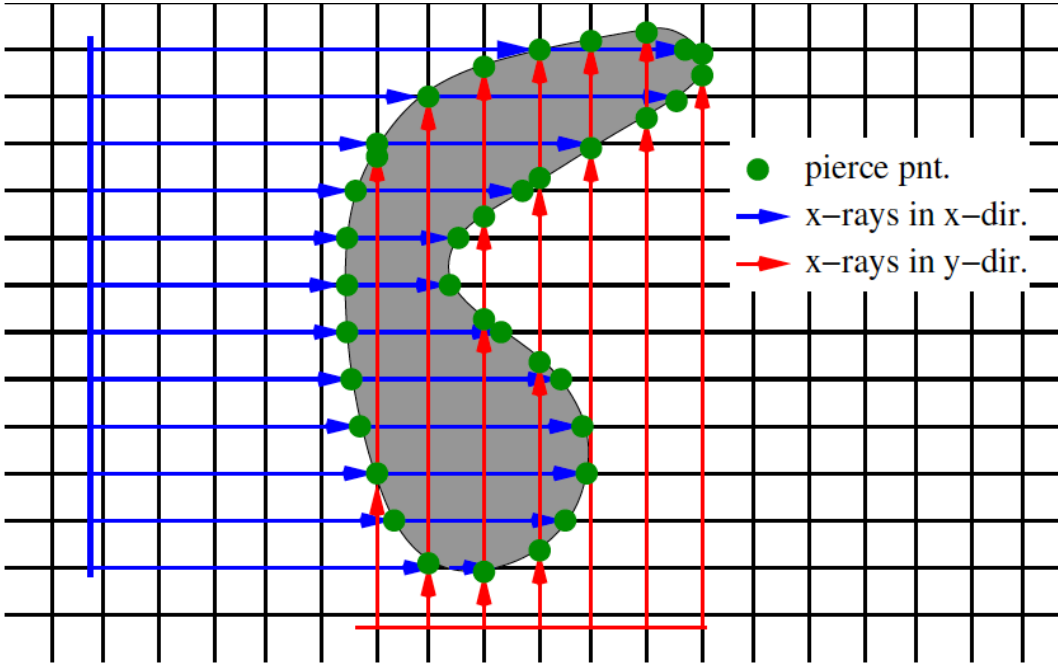


X-Ray Tracing Algorithm:

- Use discrete triangulations instead of level-set functions
- Using an optimized bounding volume hierarchy (BVH) based ray-tracing method [thanks to Intel's Embree and Tim Sandstrom]

Identification of Trapped Points:

- Occur in gaps that are smaller than irregular stencil size
- Current treatment is to reduce order of accuracy in the relevant direction

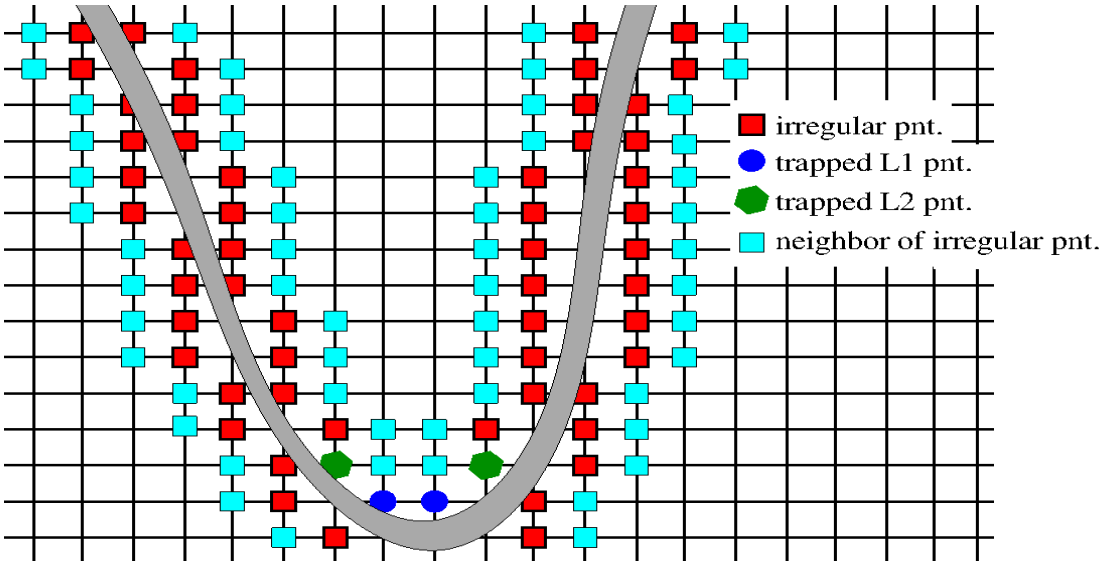

# IB Challenges for Moving Boundary Problems

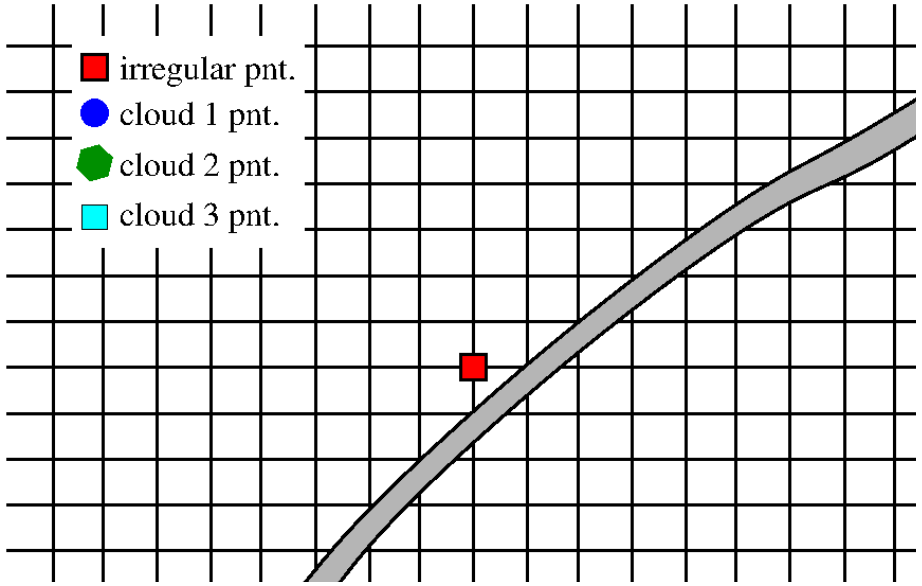


Point Cloud Selection:

- Current method does not use ghosts
- Graph walking for stencil clouds: Full clouds are build up from individual clouds at irregular points (reduces number of intersection tests)

# IB Challenges for Moving Boundary Problems

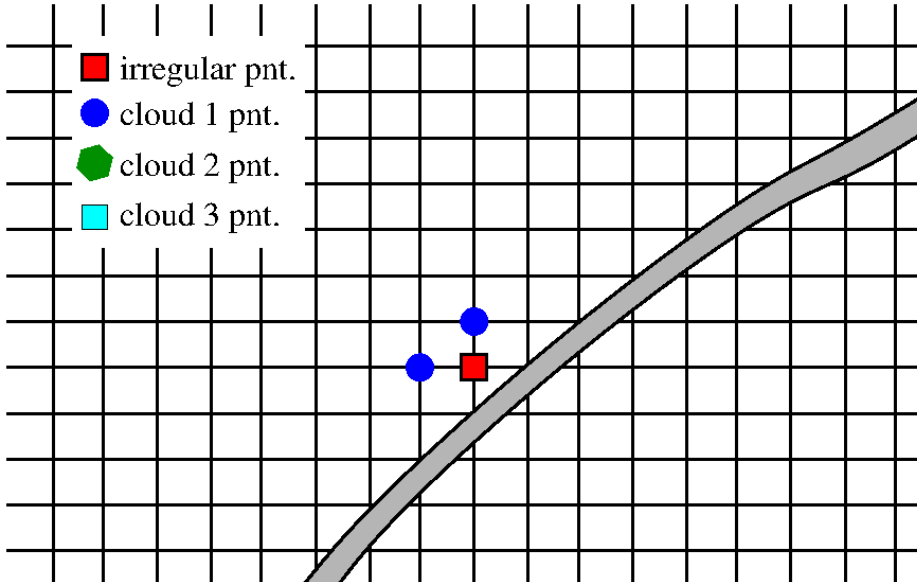


Point Cloud Selection:

- Current method does not use ghosts
- Graph walking for stencil clouds: Full clouds are build up from individual clouds at irregular points (reduces number of intersection tests)

# IB Challenges for Moving Boundary Problems

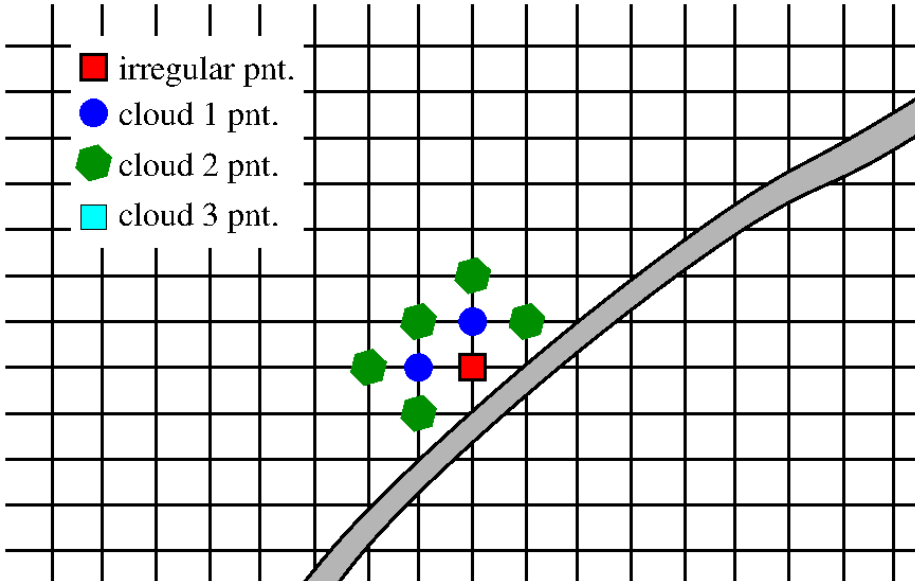


Point Cloud Selection:

- Current method does not use ghosts
- Graph walking for stencil clouds: Full clouds are build up from individual clouds at irregular points (reduces number of intersection tests)

# IB Challenges for Moving Boundary Problems

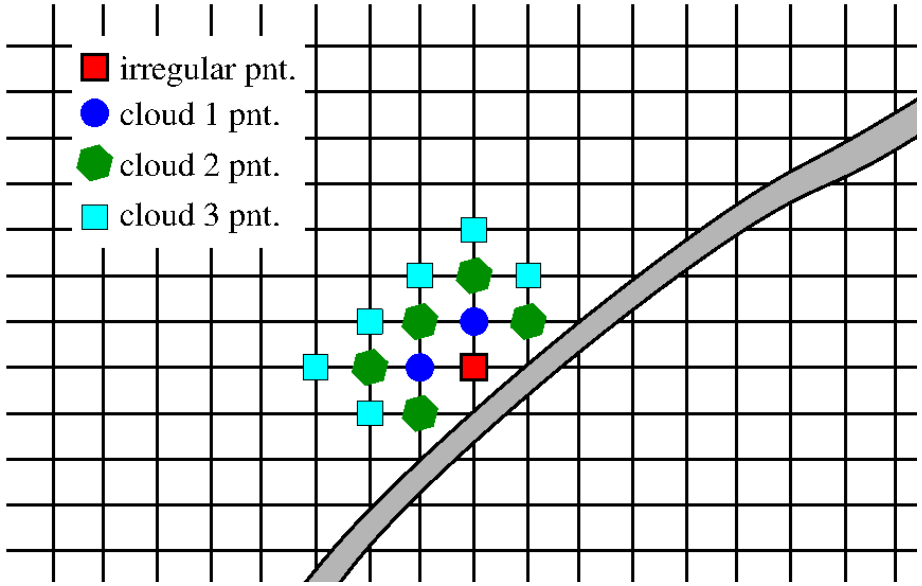


Point Cloud Selection:

- Current method does not use ghosts
- Graph walking for stencil clouds: Full clouds are build up from individual clouds at irregular points (reduces number of intersection tests)

# IB Challenges for Moving Boundary Problems

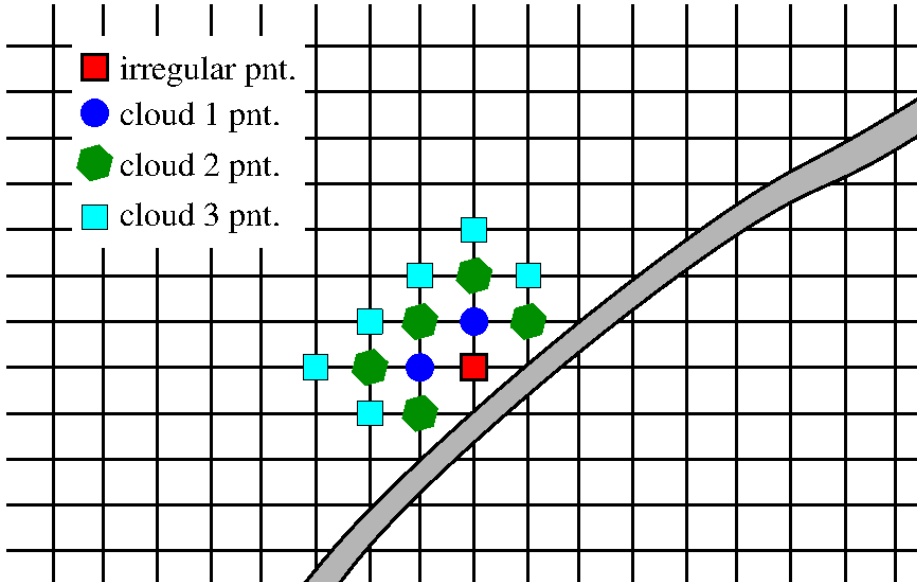


Point Cloud Selection:

- Current method does not use ghosts
- Graph walking for stencil clouds: Full clouds are build up from individual clouds at irregular points (reduces number of intersection tests)

Freshly-Cleared Cells (FCC):

- Invalid time history at FCC
- Utilize neighboring information to update data in FCC (exclude other FCCs in point cloud), ie backfilling with least-squares + BC.
- More advanced approaches are being considered

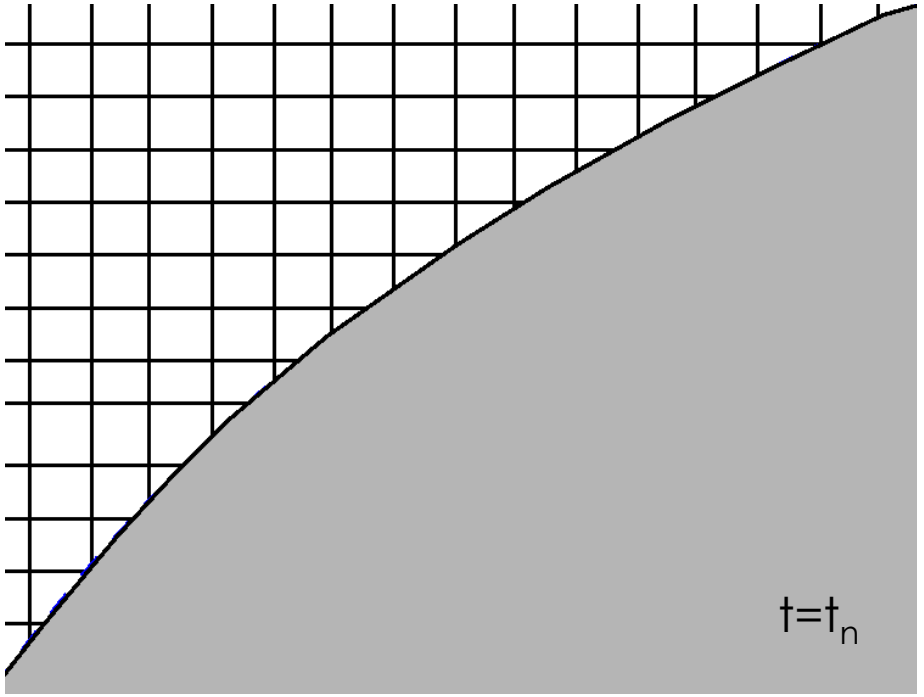

# IB Challenges for Moving Boundary Problems

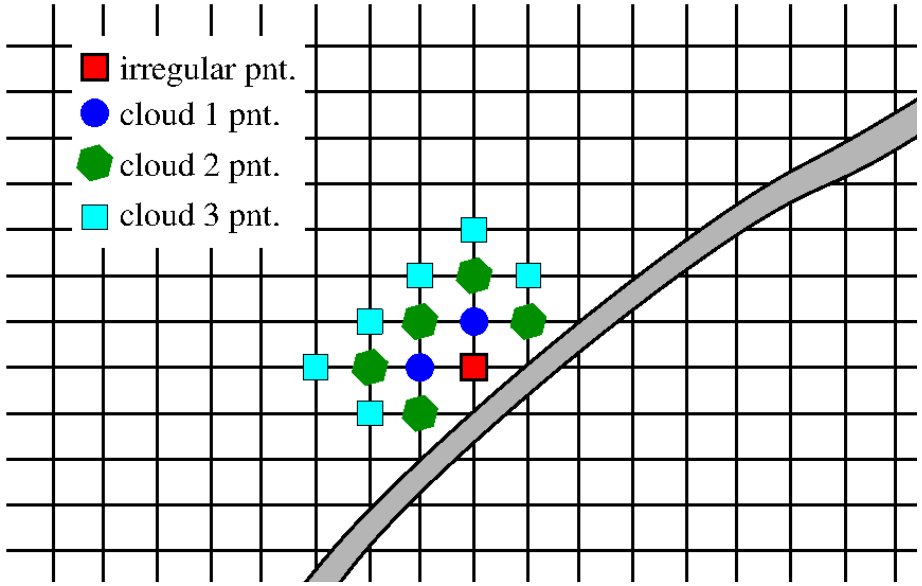


Point Cloud Selection:

- Current method does not use ghosts
- Graph walking for stencil clouds: Full clouds are build up from individual clouds at irregular points (reduces number of intersection tests)

Freshly-Cleared Cells (FCC):

- Invalid time history at FCC
- Utilize neighboring information to update data in FCC (exclude other FCCs in point cloud), ie backfilling with least-squares + BC.
- More advanced approaches are being considered

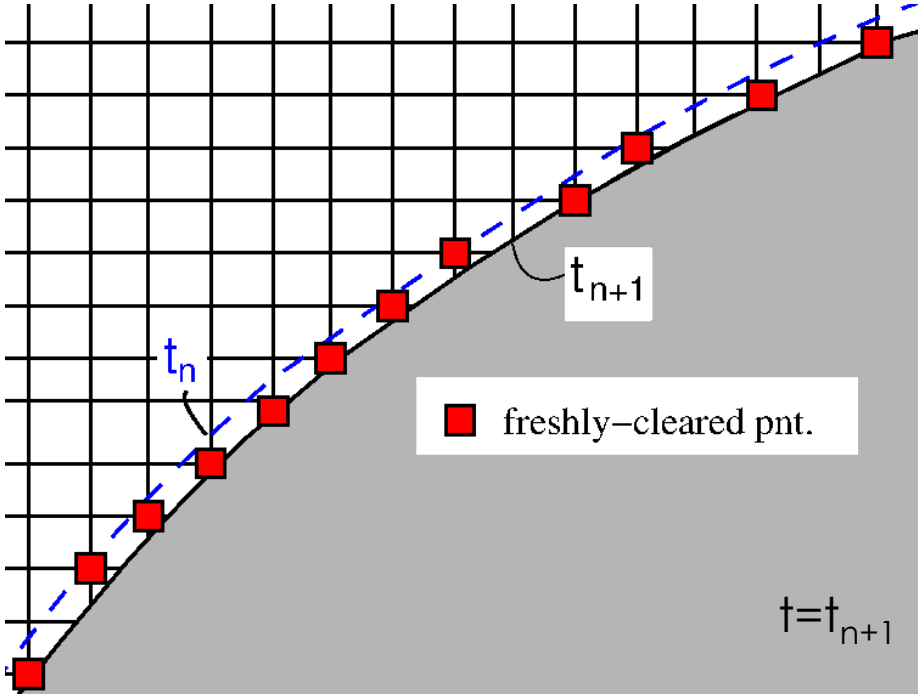

# Viscous Wall Treatment at High Reynolds Number

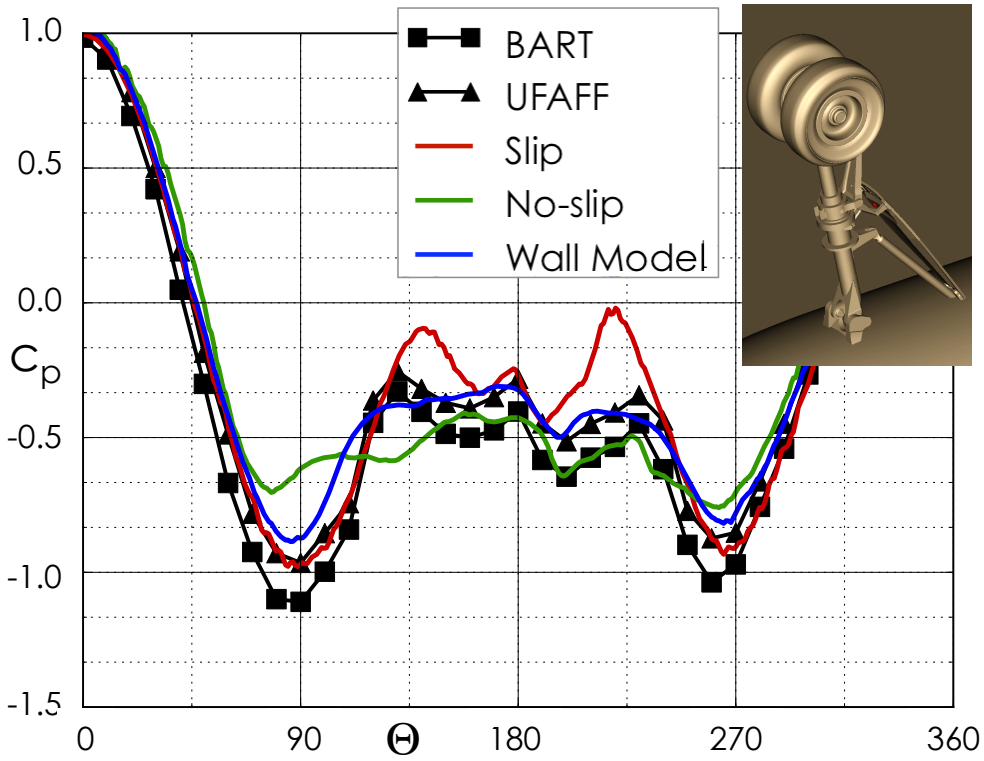


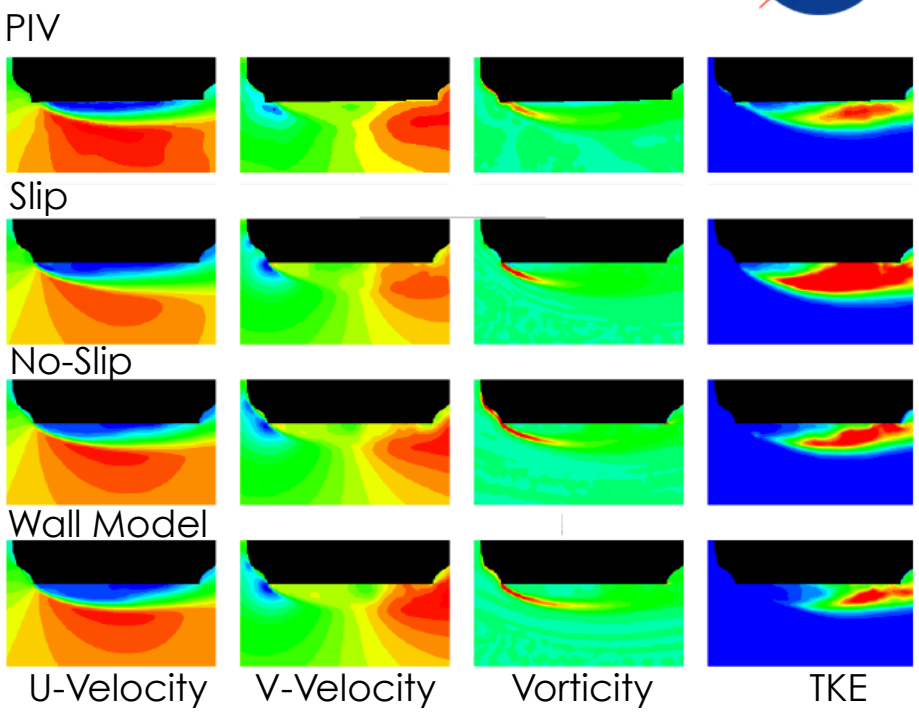


- Utilize wall model to mimic effect of viscous wall
- No-slip separates too early and slip wall stays attached all the way
- Viscous wall treatment is an ongoing research topic

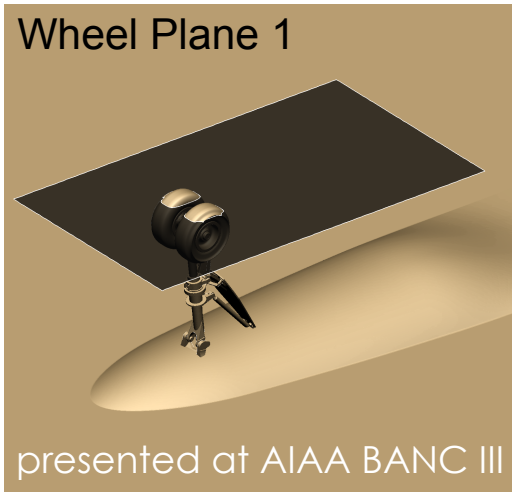

# Outline


1. Introduction to Acoustic Analysis of Contra Rotating Open Rotor
2. Numerical Methods
3. Computational and Experimental Setups
4. Comparison with Experiments
5. Brief Analysis Acoustic Near-Field for High and Low Speed Cases
6. Summary

# Flow Conditions

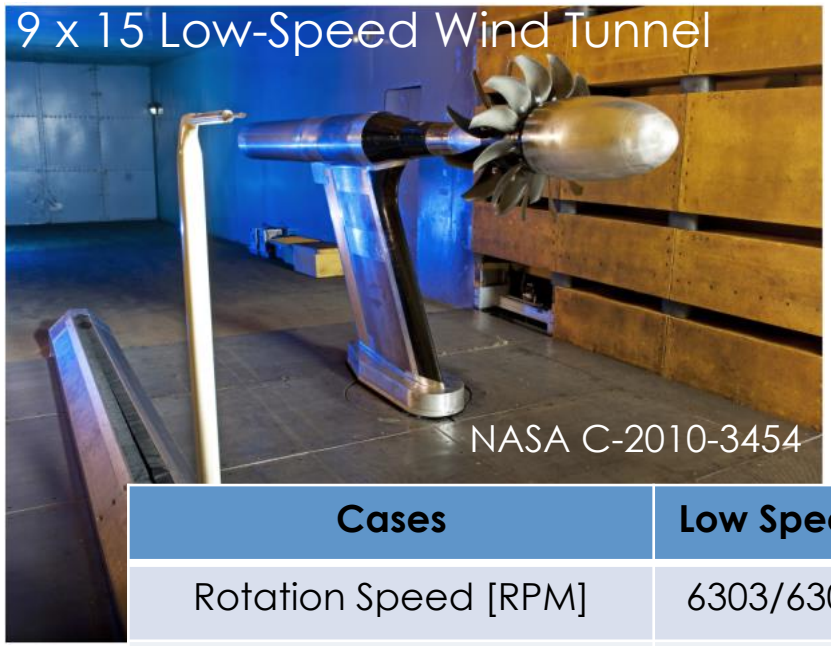


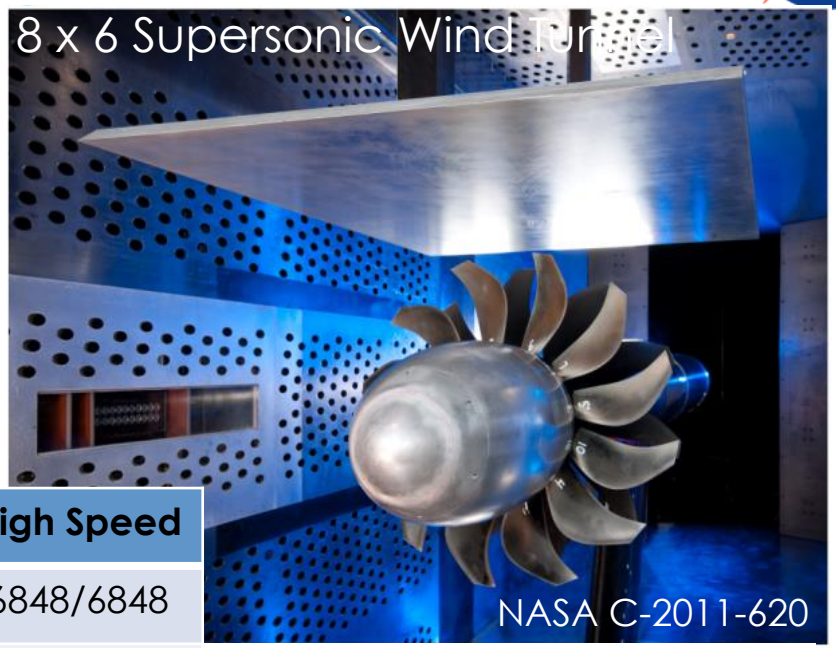


| Cases | Low Speed | High Speed |
|---|---|---|
| Rotation Speed [RPM] | 6303/6303 | 6848/6848 |
| Blade Setting (fwd/aft) [°] | 40.1/40.8 | 64.4/61.8 |
| Mach | 0.20 | 0.78 |

Pressure Sensors


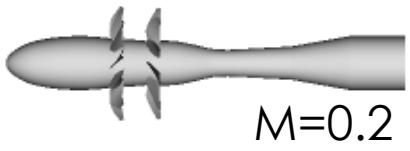


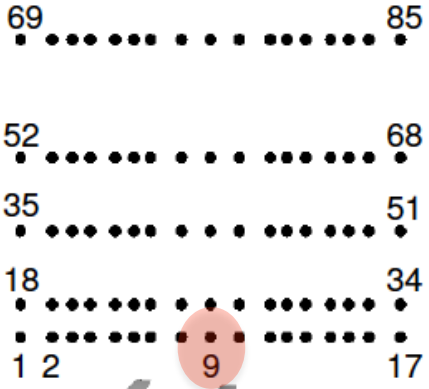


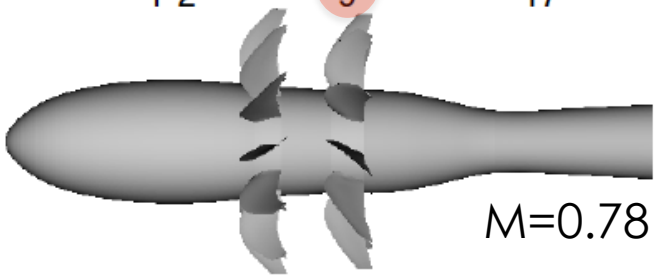

# Computational Setup

Block Structured Cartesian Mesh

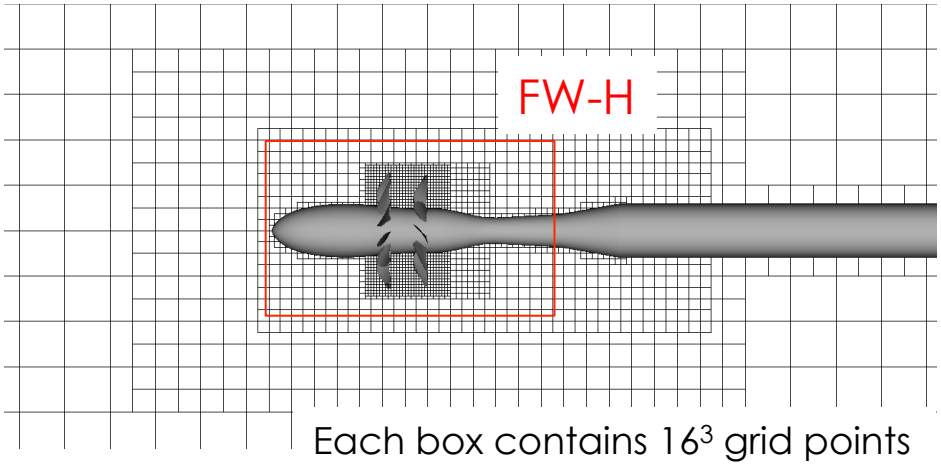


- Higher-order shock capturing scheme: modified ZWENO6
  (Brehm, Barad, Housman, and Kiris, CAF-2015)
- $4^{th}$-order explicit RK time-integration with $\Delta t$ defined through CFL≈1
- Implicit large eddy simulation based on previous experience with jet impingement problem

Grid Refinement Study for M=0.2:

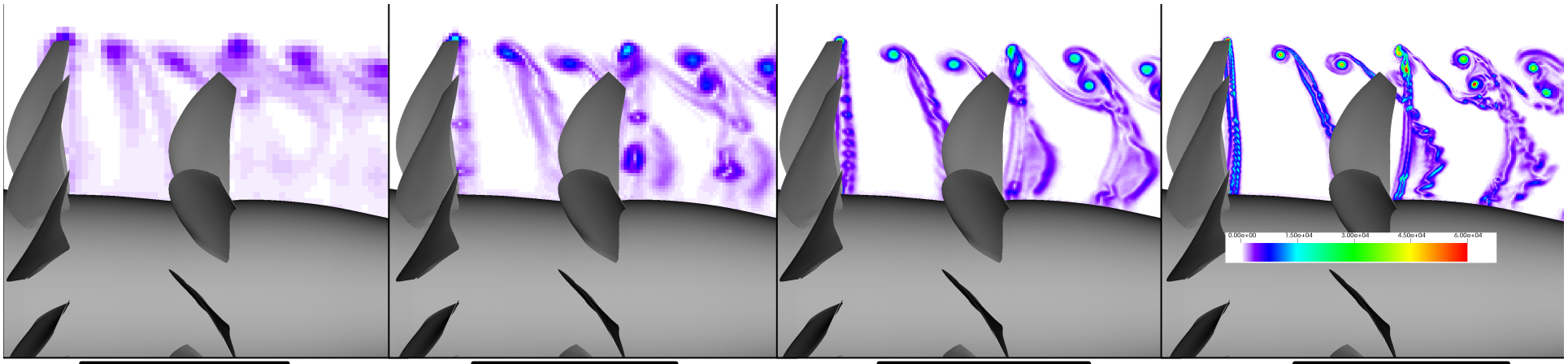

| 8 Levels: | 9 Levels: | 10 Levels: | 11 Levels: |
|---|---|---|---|
| $\Delta x_{min}$=8e-3 | $\Delta x_{min}$=4e-3 | $\Delta x_{min}$=2e-3 | $\Delta x_{min}$=1e-3 |
| $N_{tot}$=65M | $N_{tot}$=110M | $N_{tot}$=160M | $N_{tot}$=350M |

# Unsteady Flow Field – Passive Particle Viz

Low Speed

High Speed

# Outline


1. Introduction to Acoustic Analysis of Contra Rotating Open Rotor
2. Numerical Methods
3. Computational and Experimental Setups
4. Comparison with Experiments
5. Brief Analysis Acoustic Near-Field for High and Low Speed Cases
6. Summary

# Comparison With Experiments (Low Speed)

Velocity Magnitude Contours

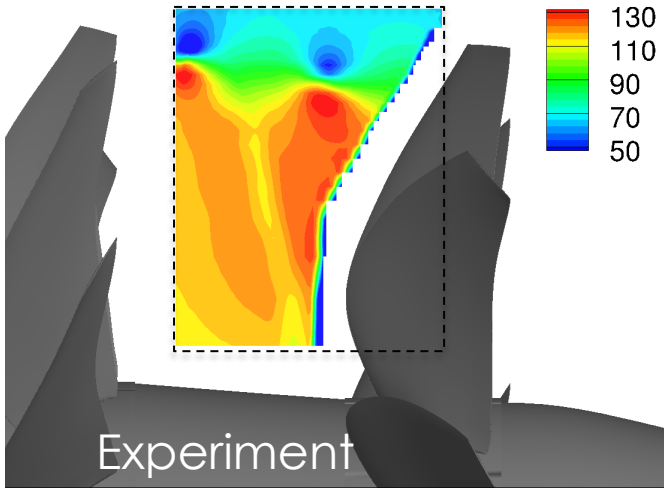


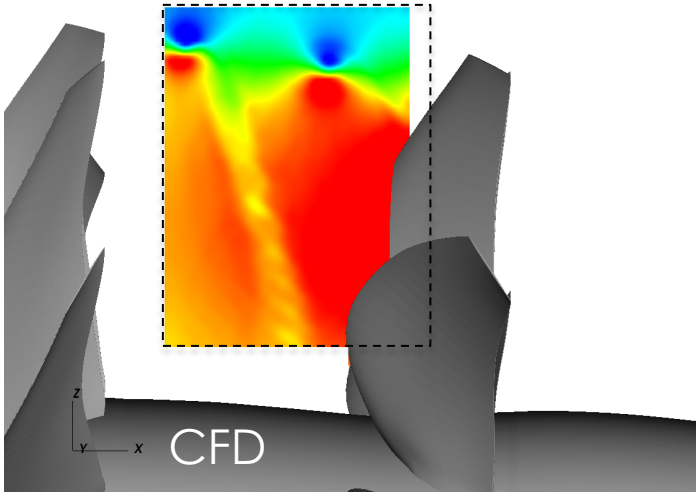


Iso-surface of velocity magnitude with $|v|/v_\infty$=0.84 (**red**) and 1.91 (**blue**)

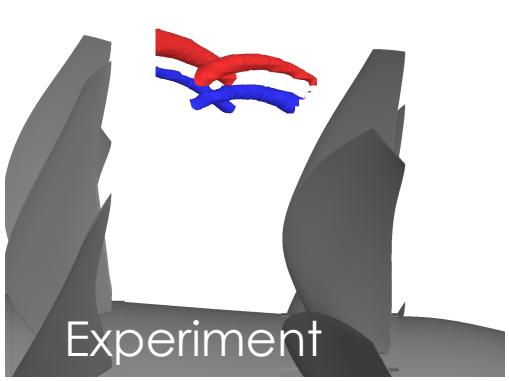


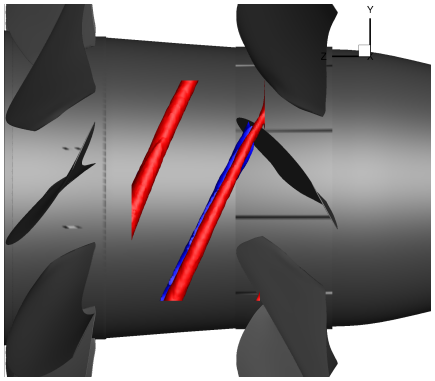

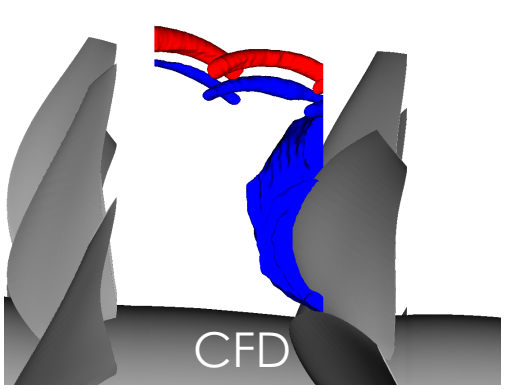


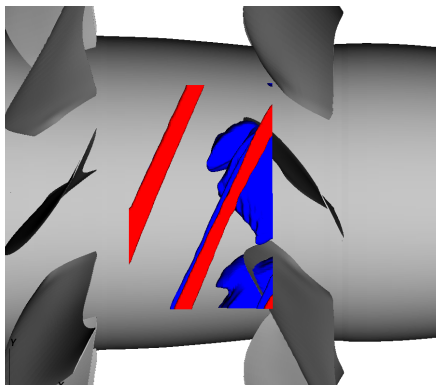

- Good agreement of velocity magnitude contours with experiment
- Evolution of tip vortices seems to be well captured

# Thrust Comparison

Low Speed

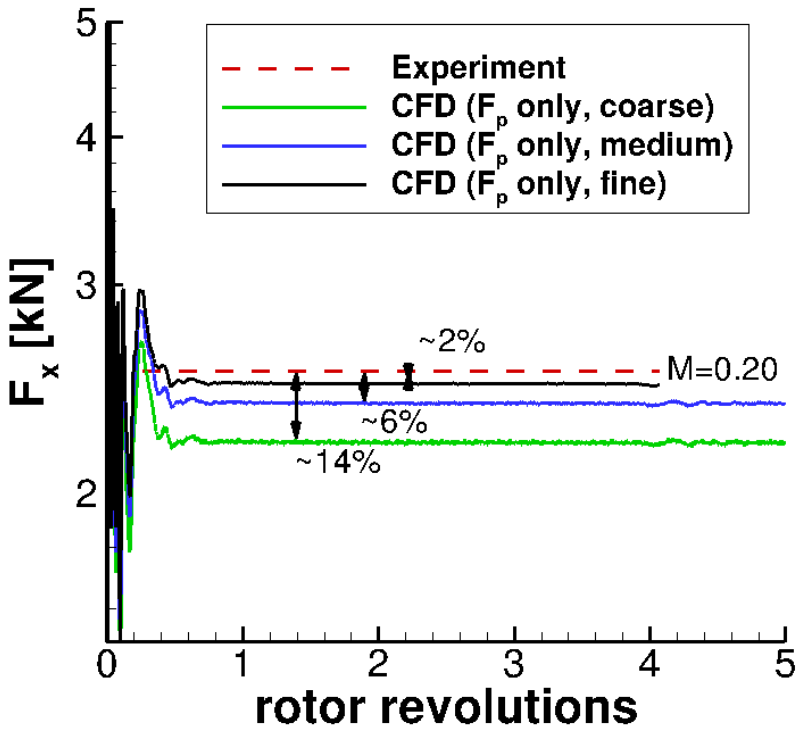


High Speed

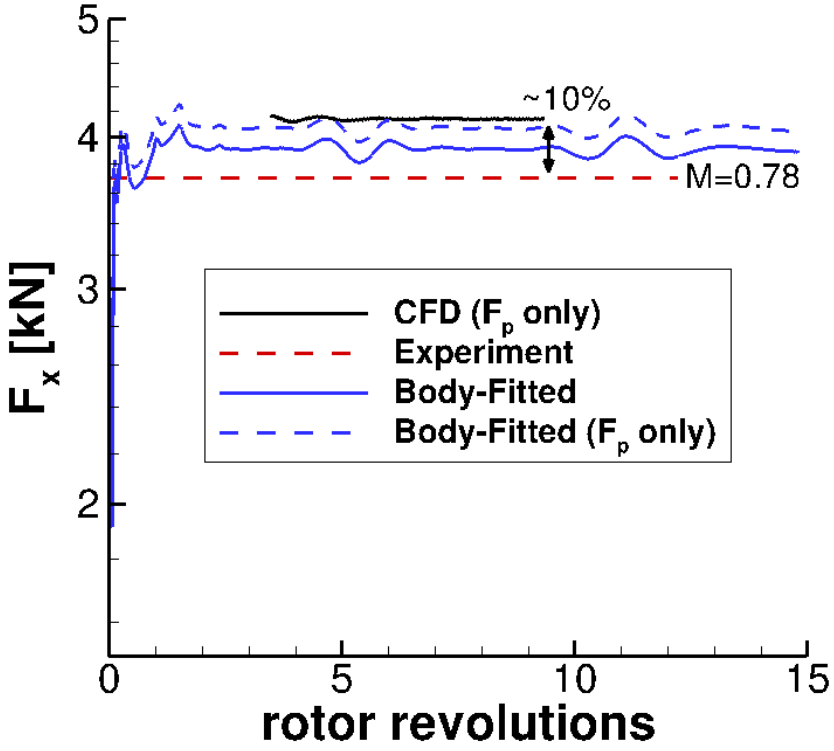


- Note that only pressure drag was considered (ratio 4:100 for M=0.78)
- Fluctuations in thrust values for LAVA-Curvilinear are due to reflections at outflow boundaries
- Agreement with experiment is in the range of other computations (LAVA-Curvilinear, Overflow, and *FINE™/Turbo*)

# Far-Field Spectra

Low Speed (at Probe 9)

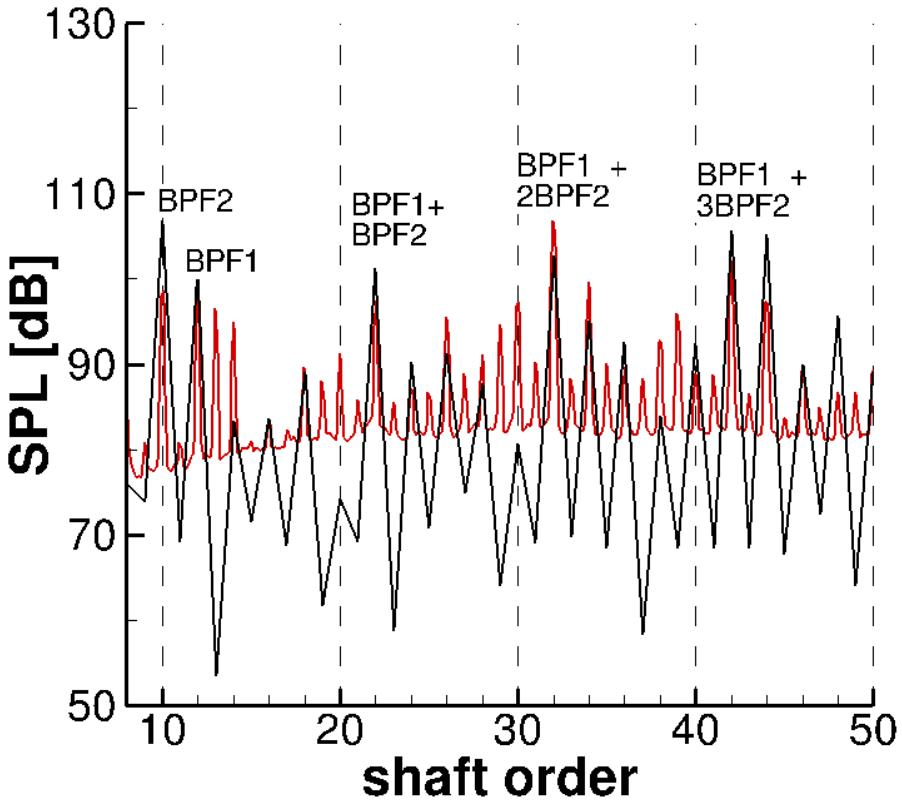


High Speed (at Probe 9)

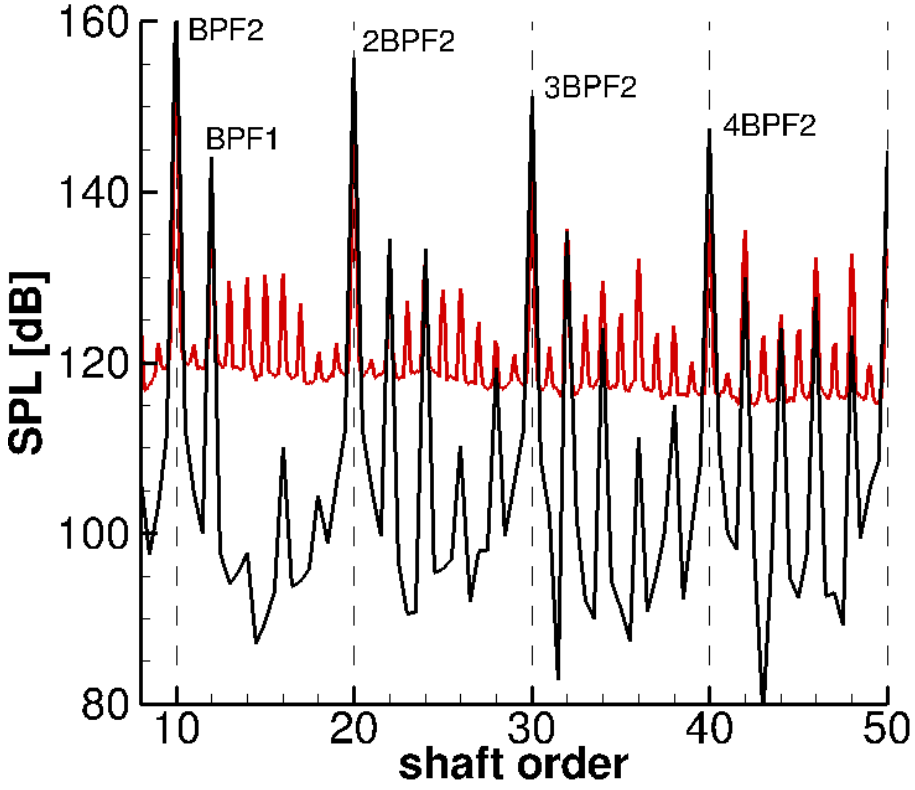


- BPF = blade passing frequency
- Shaft order (SO) = frequency/shaft rotation rate

# Far-Field Spectra

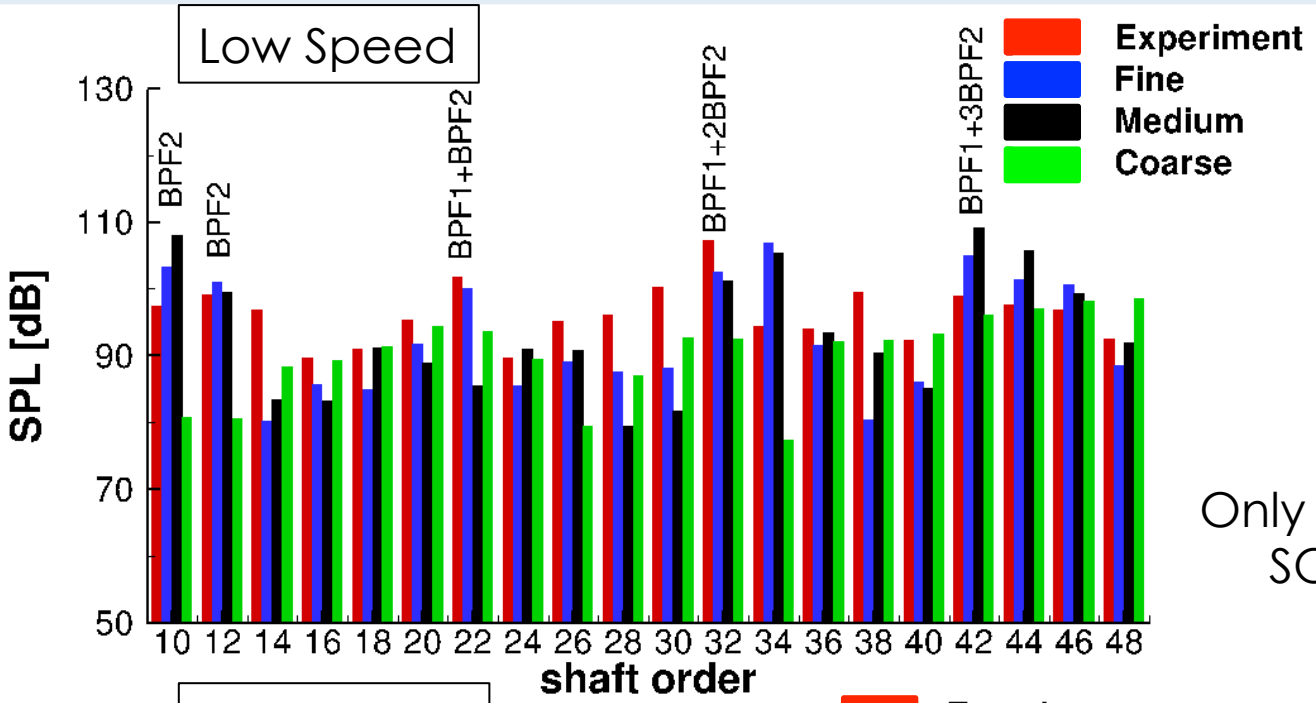


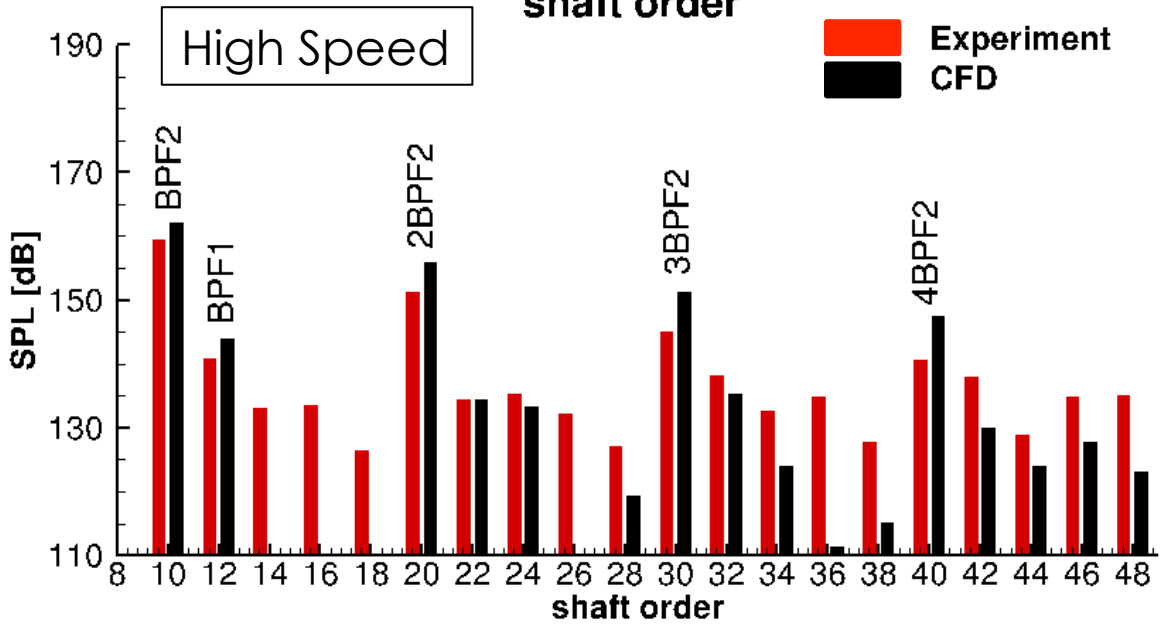


Only consider tones with SO(m,n)=12m+10n

# Plate Effect in High Speed Case

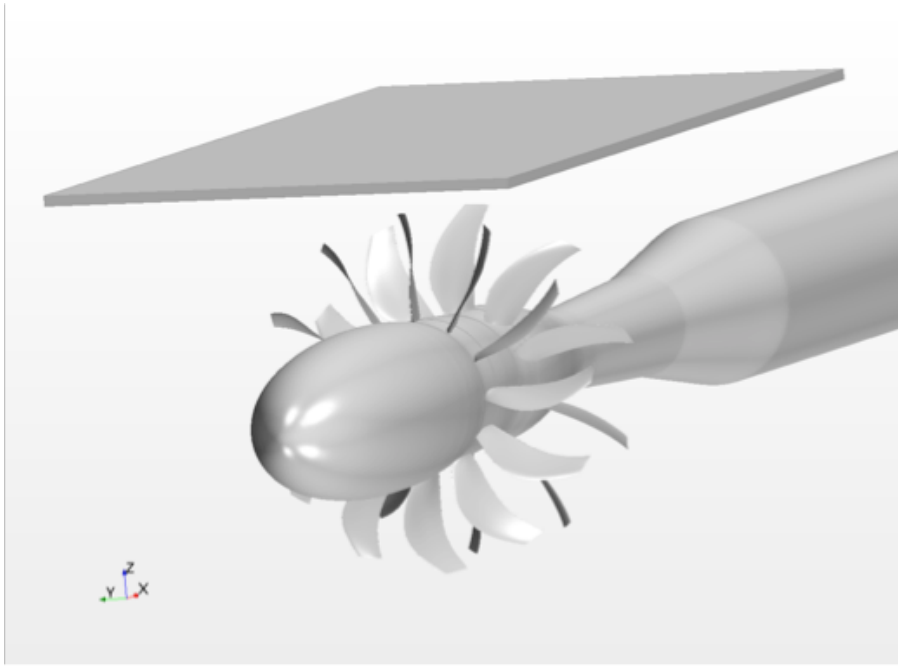

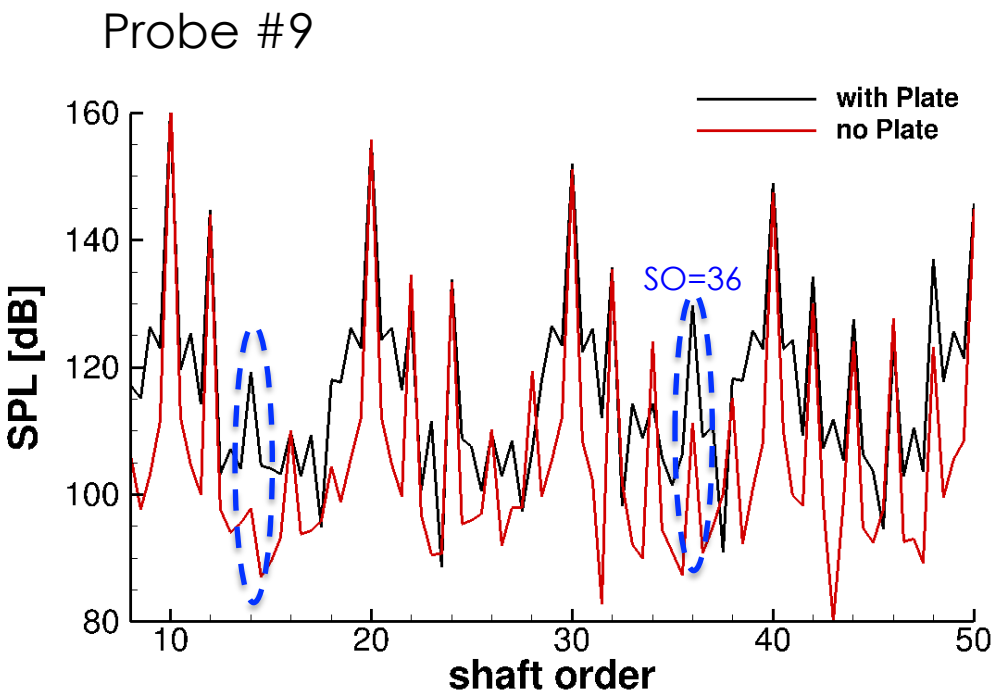


- Plate effect was accounted for by assuming perfect reflection ($6dB=10\log_{10}(2^2)$)
- Simulation with plate at first row of acoustic sensors
- Numerical simulations results with plate show odd tones
- Plate affects broadband noise level
- Plate does not affect the most dominant tones

# Spatial Dependence Of Tones (Low Speed)

Fundamental Tones

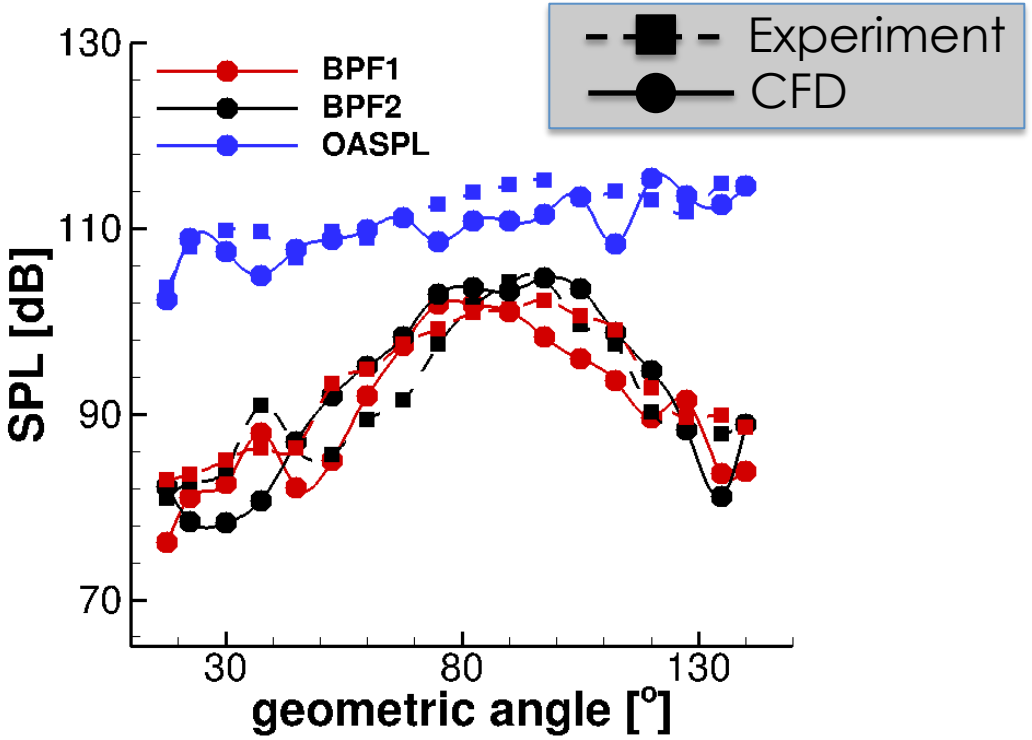


Grid Resolution Study

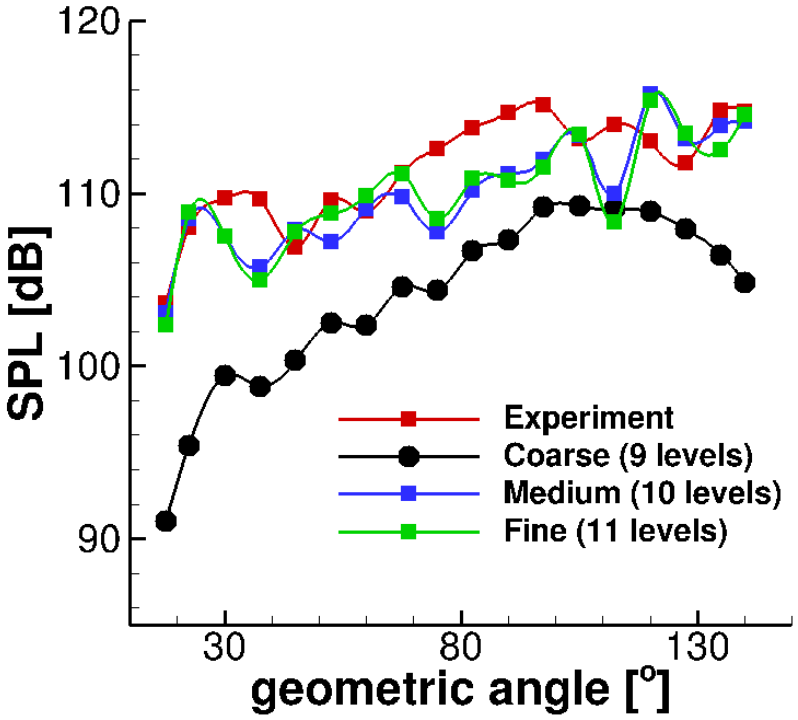


- Fundamental tones decay rapidly away from the blades
- OASPL is increasing with increasing geometric angle
- Small difference in OASPL for fine and medium mesh

# Spatial Dependence Of Tones (Low Speed)

Fundamental Tones

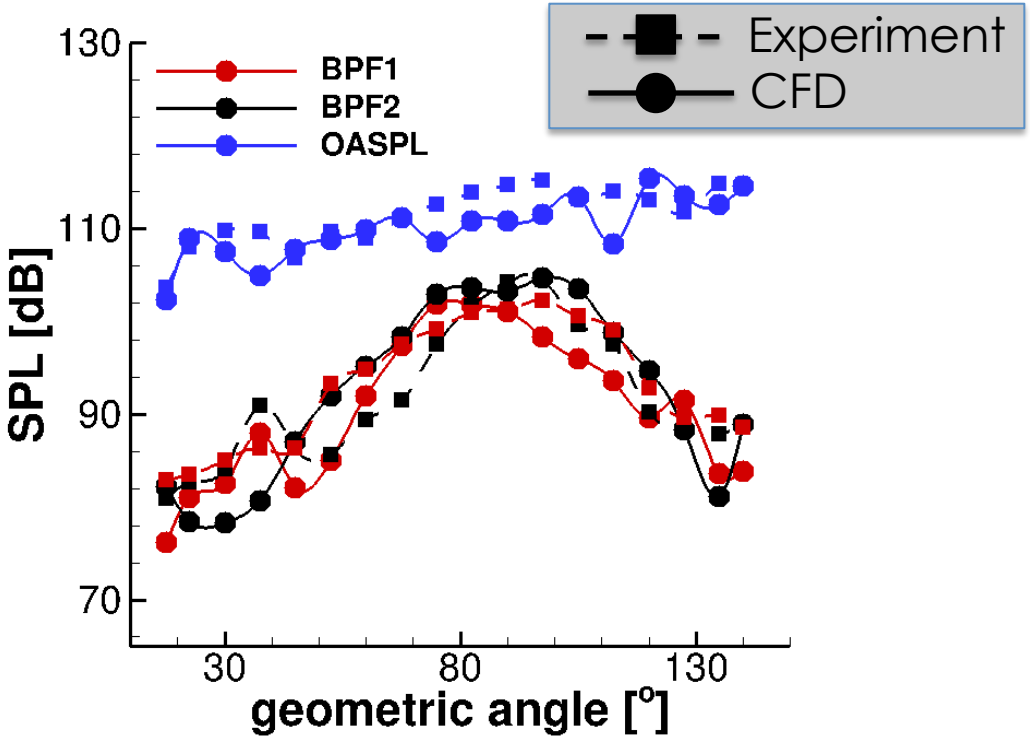


Higher-Order Interactions

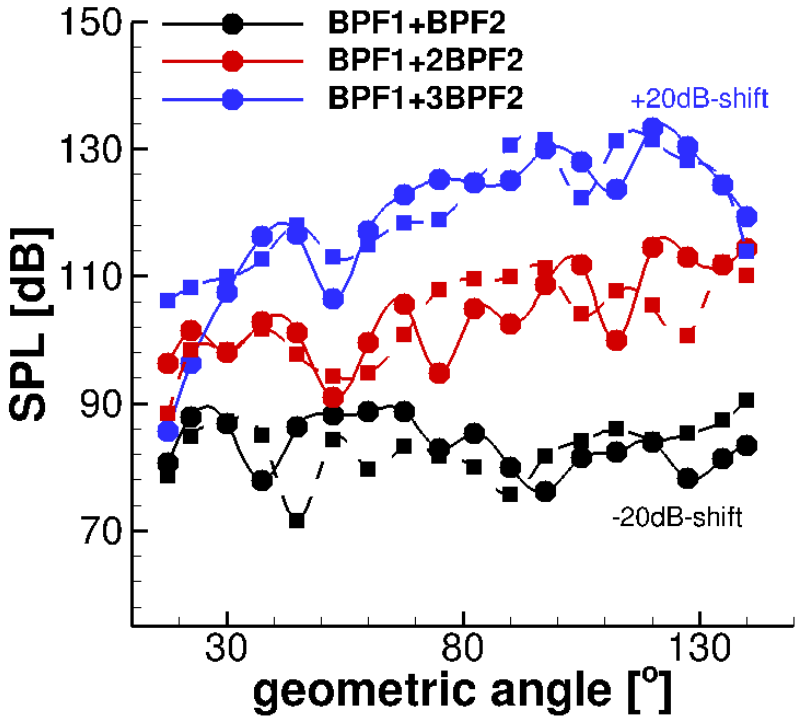


- Fundamental tones decay rapidly away from the blades
- OASPL is increasing with increasing geometric angle
- Small difference in OASPL for fine and medium mesh
- Higher-order interaction tones obtain significant amplitudes similar to fundamental tones

# Spatial Dependence Of Tones (high Speed)

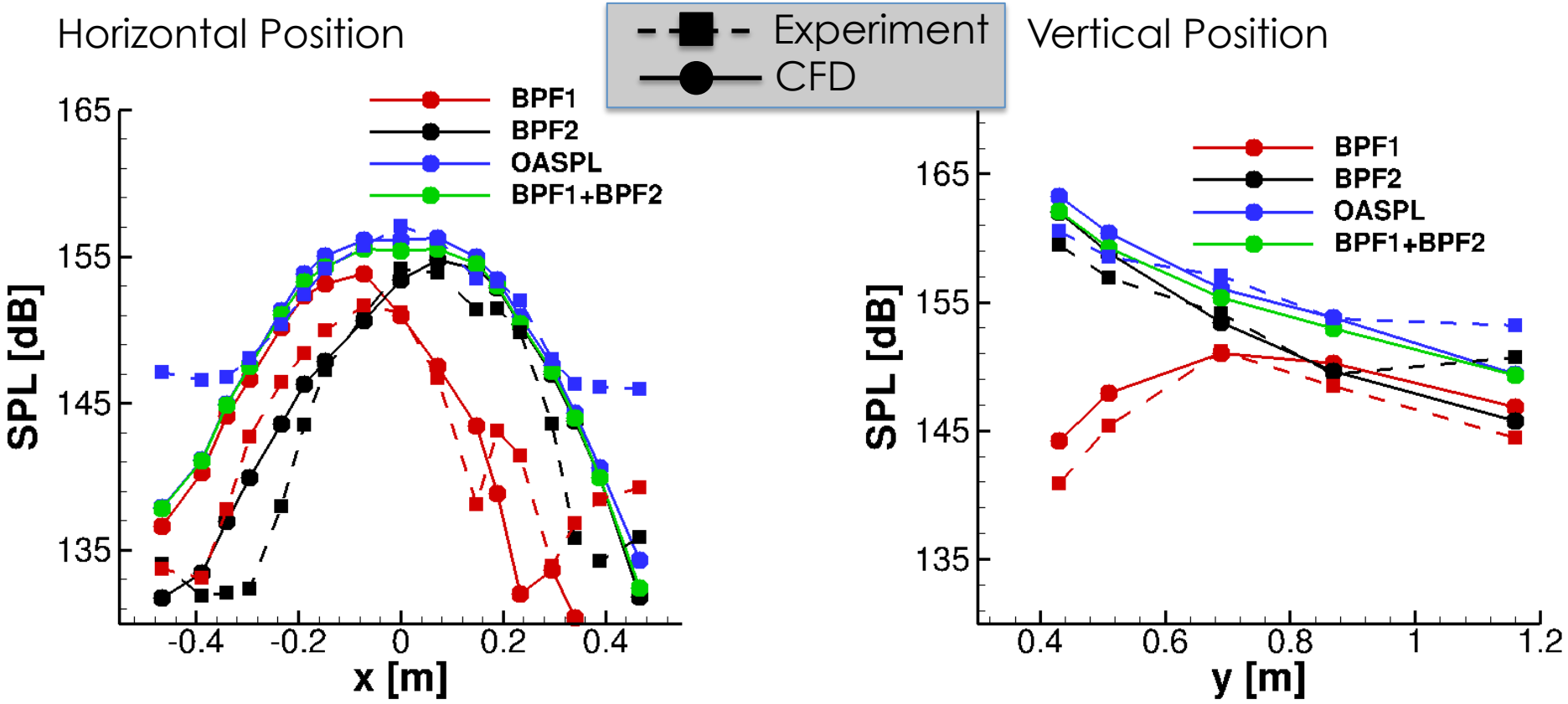


- Fundamental tones dominate OASPL
- Added tonal SPL with BPF1+BPF2 only for comparison
- General trends are well captured for low and high speed cases
- Broadband noise important at small x (<-0.4) and large x (>0.4)

# Outline

1. Introduction to Acoustic Analysis of Contra Rotating Open Rotor
2. Numerical Methods
3. Computational and Experimental Setups
4. Comparison with Experiments
5. Brief Analysis Acoustic Near-Field for High and Low Speed Cases
6. Summary

# Unsteady Flow Field – Numerical Schlieren

Low Speed

High Speed

# Near Field Acoustic Analysis (Low Speed)

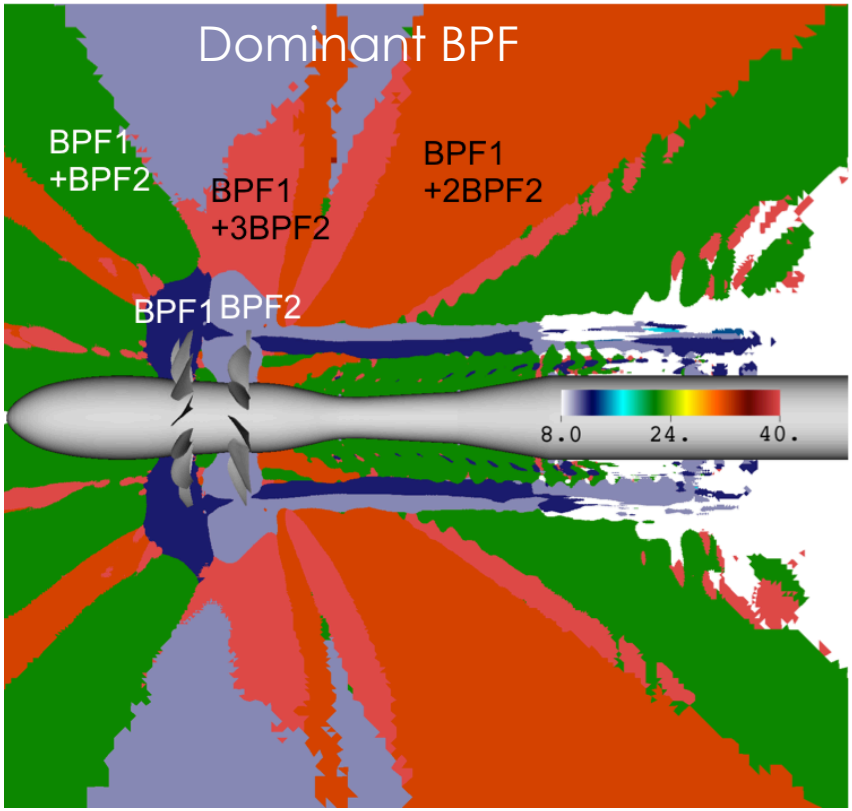


Normalized Max. Pressure Amplitude

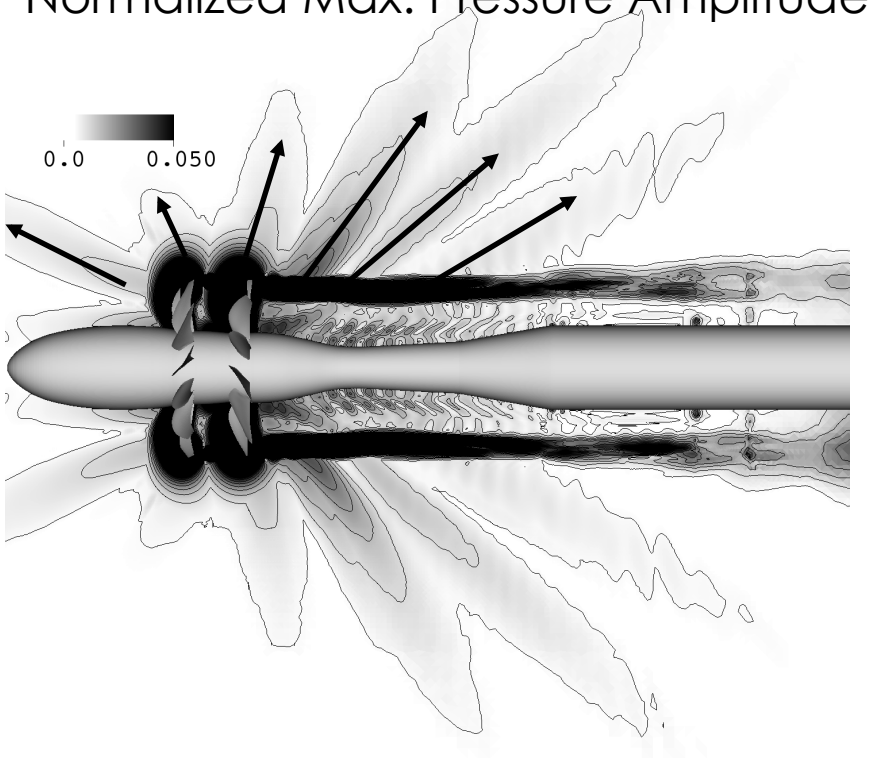


- Analysis captures acoustic waves but also hydrodynamic instability waves
- BPF1 and BPF2 are dominant in a very small region around the rotors and along the tip vortices
- Various higher-order interactions play an important role

# Near Field Acoustic Analysis (High Speed)

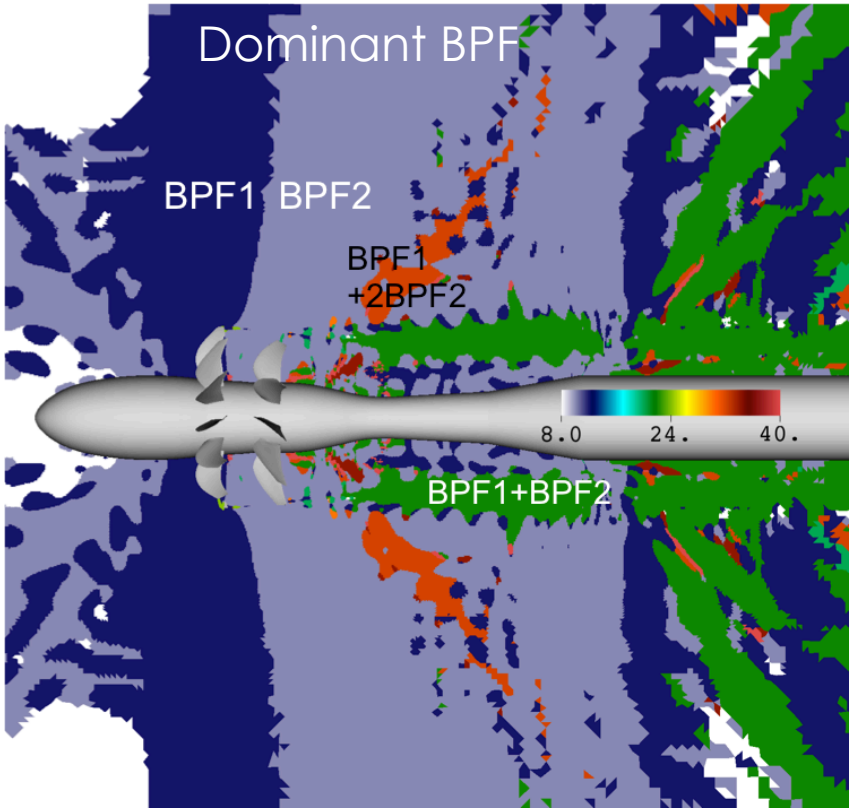


Normalized Max. Pressure Amplitude

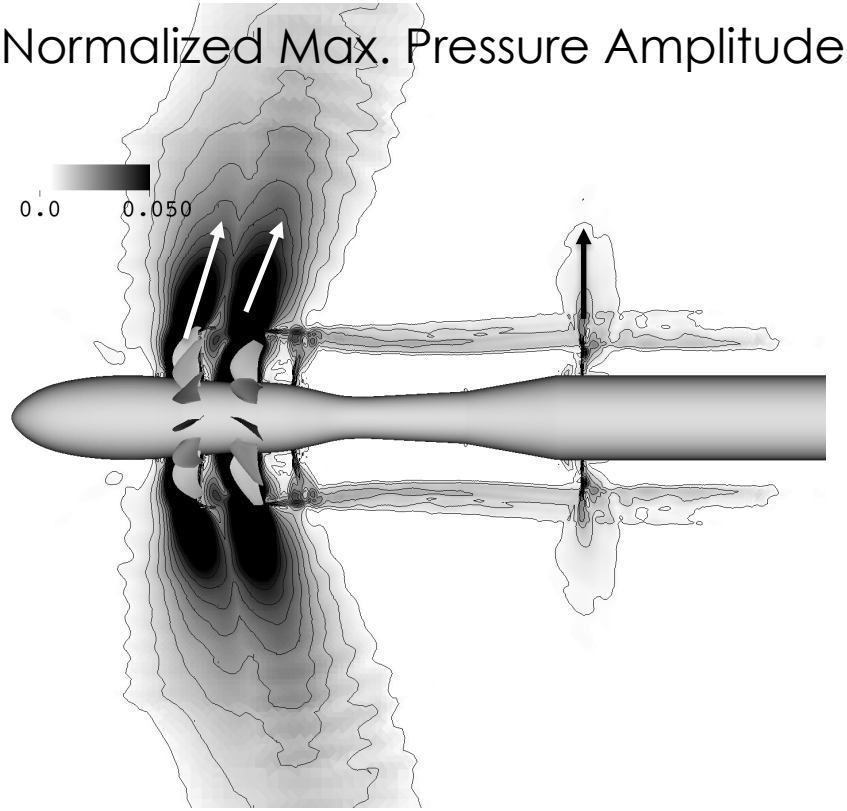


- BPF1 and BPF2 are the dominant frequencies
- BPF1+BPF2 is dominant along the tip vortices and induces unsteady shock motion that generates acoustic waves in the back

# Near Field Acoustic Analysis (BPF2)

Low Speed

High Speed

amplitude

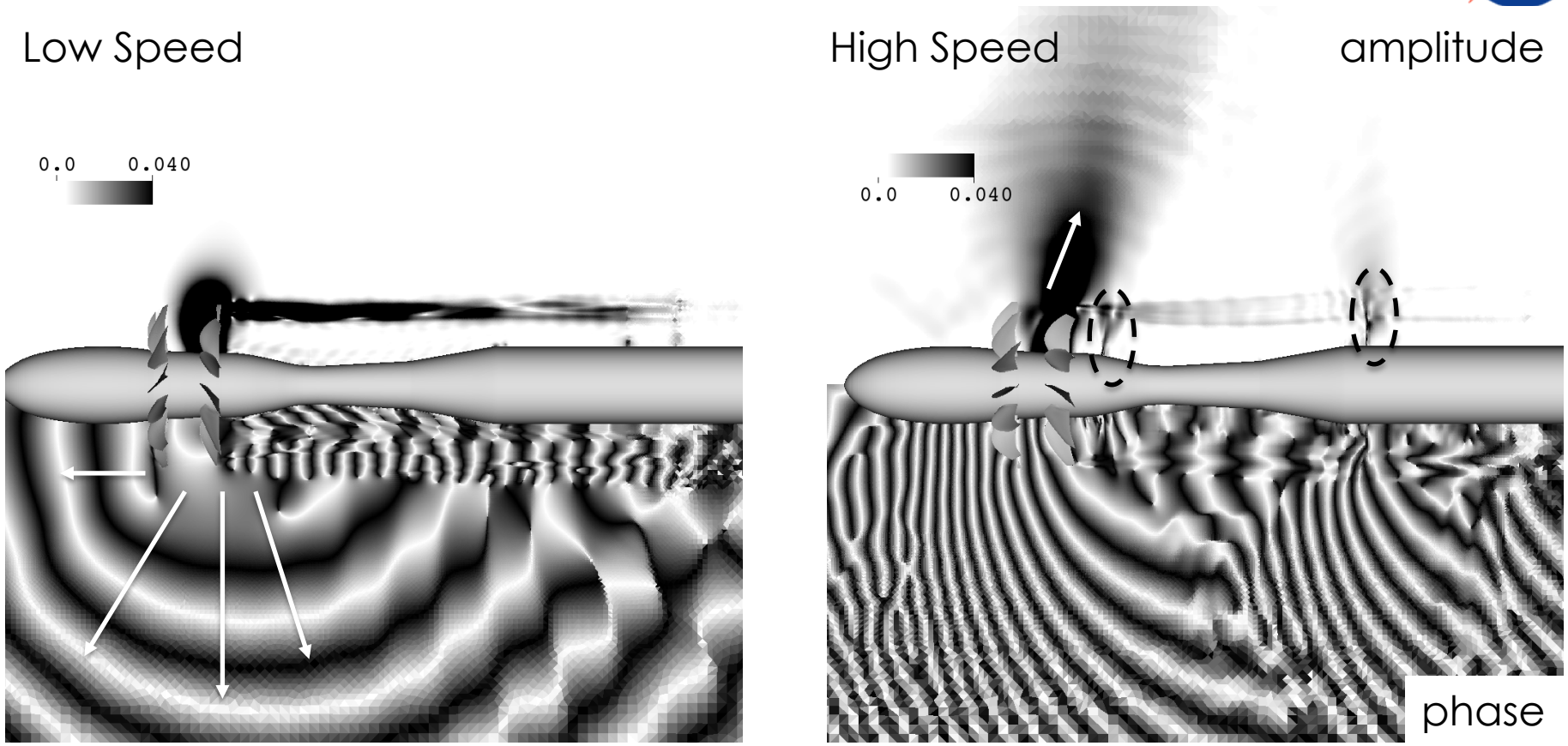


- BPF2 amplitude is dominant in small region around rotor for M=0.3 while strong acoustic waves radiate away from the front rotor for M=0.78
- BPF2 remains dominant along the tip vortices for M=0.2
- Similar observations for BPF1

# Near Field Acoustic Analysis (BPF1+BPF2)

Low Speed

High Speed

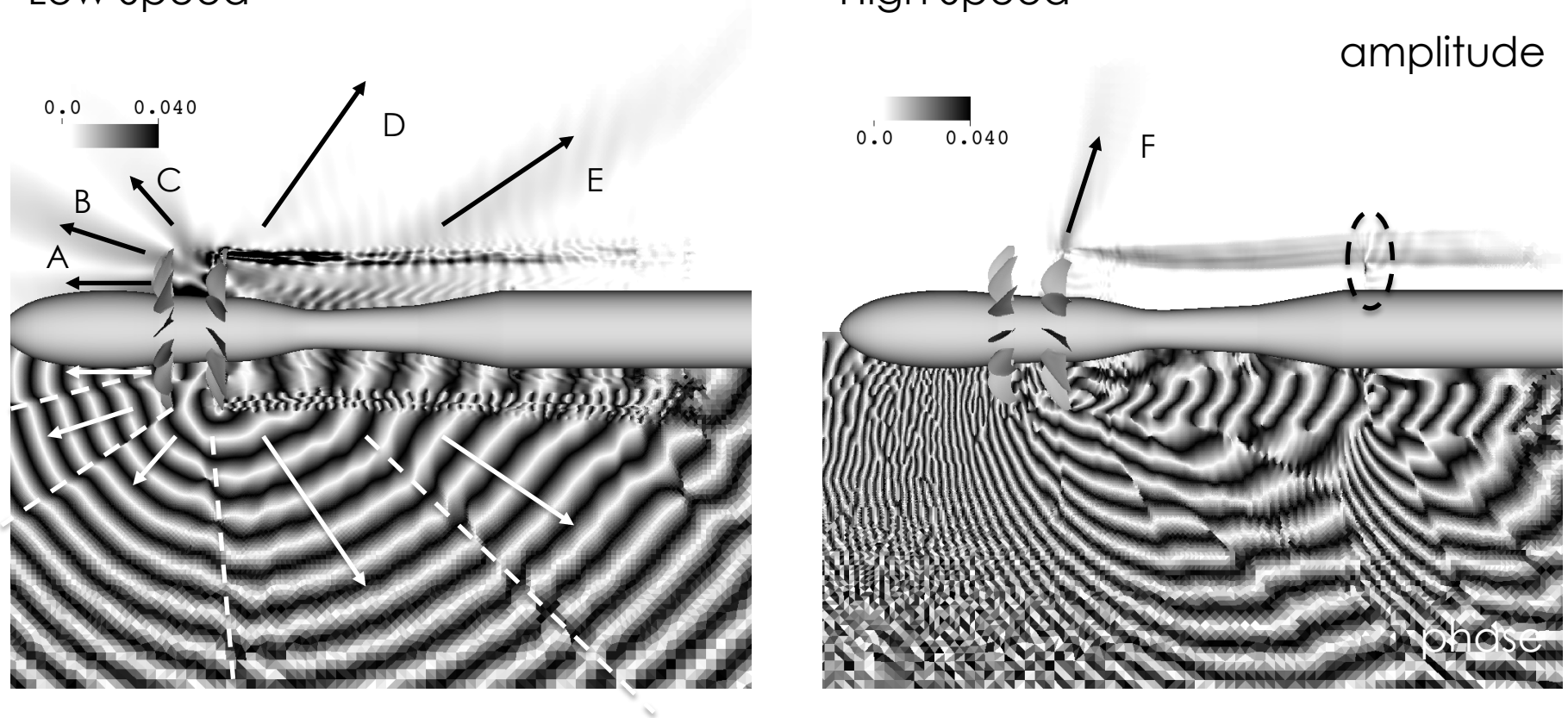


- Interaction of rear rotor with tip vortex from front rotor generates BPF1+BPF2 tone (C, D & F)
- Region B appears to originate from midsection of rear rotor
- Region E originates from the wake and plays dominant role for large geometric angles

# Outline

1. Introduction to Acoustic Analysis of Contra Rotating Open Rotor
2. Numerical Methods
3. Computational and Experimental Setups
4. Comparison with Experiments
5. Brief Analysis Acoustic Near-Field for High and Low Speed Cases
6. Summary

# Summary

- LAVA's sharp immersed boundary (IB) method was used to simulate flow around a contra-rotating open rotor for nominally takeoff and cruise conditions
- Key issues for simulating moving boundaries with IB were addressed:
  - Treatment of freshly cleared cells
  - Efficient geometry queries
  - Efficient computation of irregular stencils (every time-step!)
  - Treatment of thin geometry:
    - Interior only scheme
    - Stencil cloud selection
    - Interpolation to thin surfaces
- Acoustic data obtained from combination of CFD near-field + FW-H method compare well with experiments
- Distinct differences in low and high speed acoustic fields
  - OASPL for M=0.78 peaks around 90° while OASPL keeps increasing with increasing geometric angle
  - High speed case is dominated by BPF1 and BPF2
  - Low speed case showed complicated higher-order interactions that are relevant for the OASPL

# Acknowledgments


- This work was supported by the NASA Advanced Air Transport Technology (AATT) project under the Advanced Air Vehicles Program (AAVP)

- Edmane Envia and Christopher Miller of NASA Glenn Research Center for information on modeling open rotor noise and meshing requirements

- Jeff Housman of NASA Ames Research Center for many fruitful discussions on modeling open rotor noise

- Tim Sandstrom (optimized ray-tracing kernels, and particle visualizations) and Patrick Moran (Schlieren visualization) of NASA Ames Research Center

- Team members of the acoustic working group

- Computer time provided by NASA Advanced Supercomputing (NAS) facility at NASA Ames Research Center

# Questions?

# Unsteady Flow Field – Passive Particle Viz

M=0.2

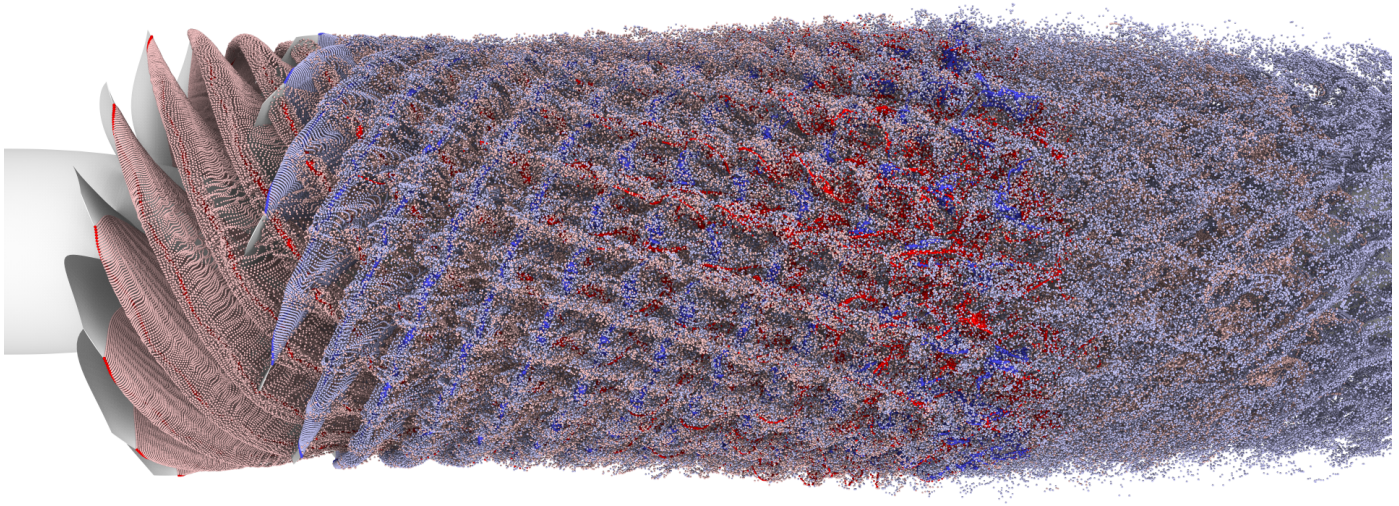

M=0.78

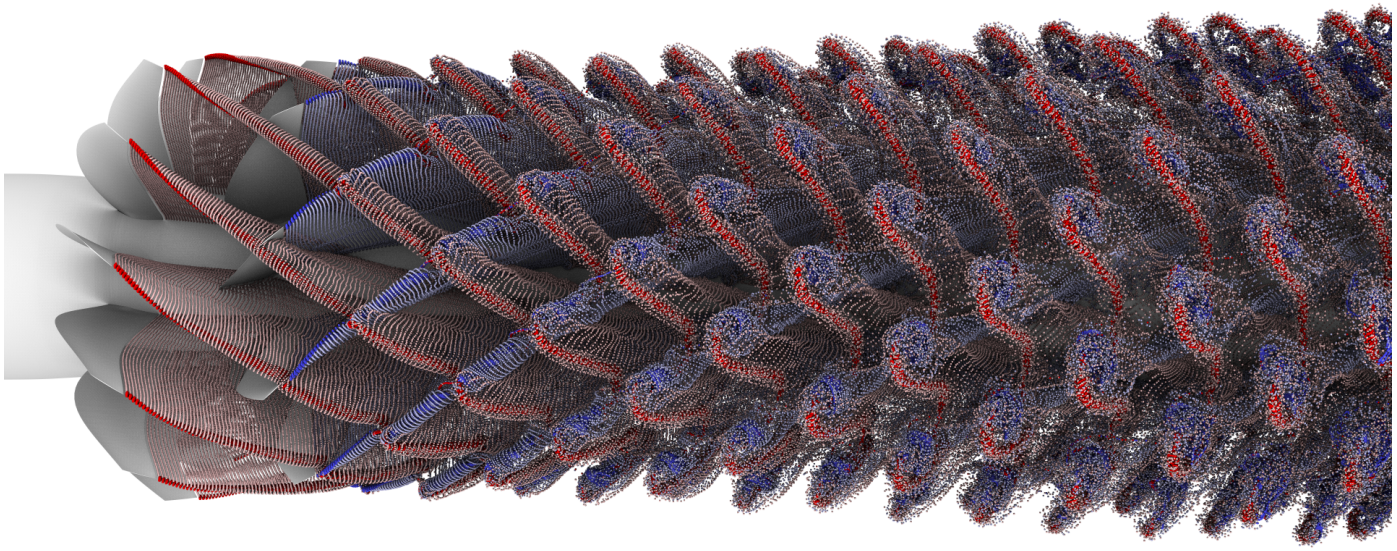

# Unsteady Flow Field – Numerical Schlieren

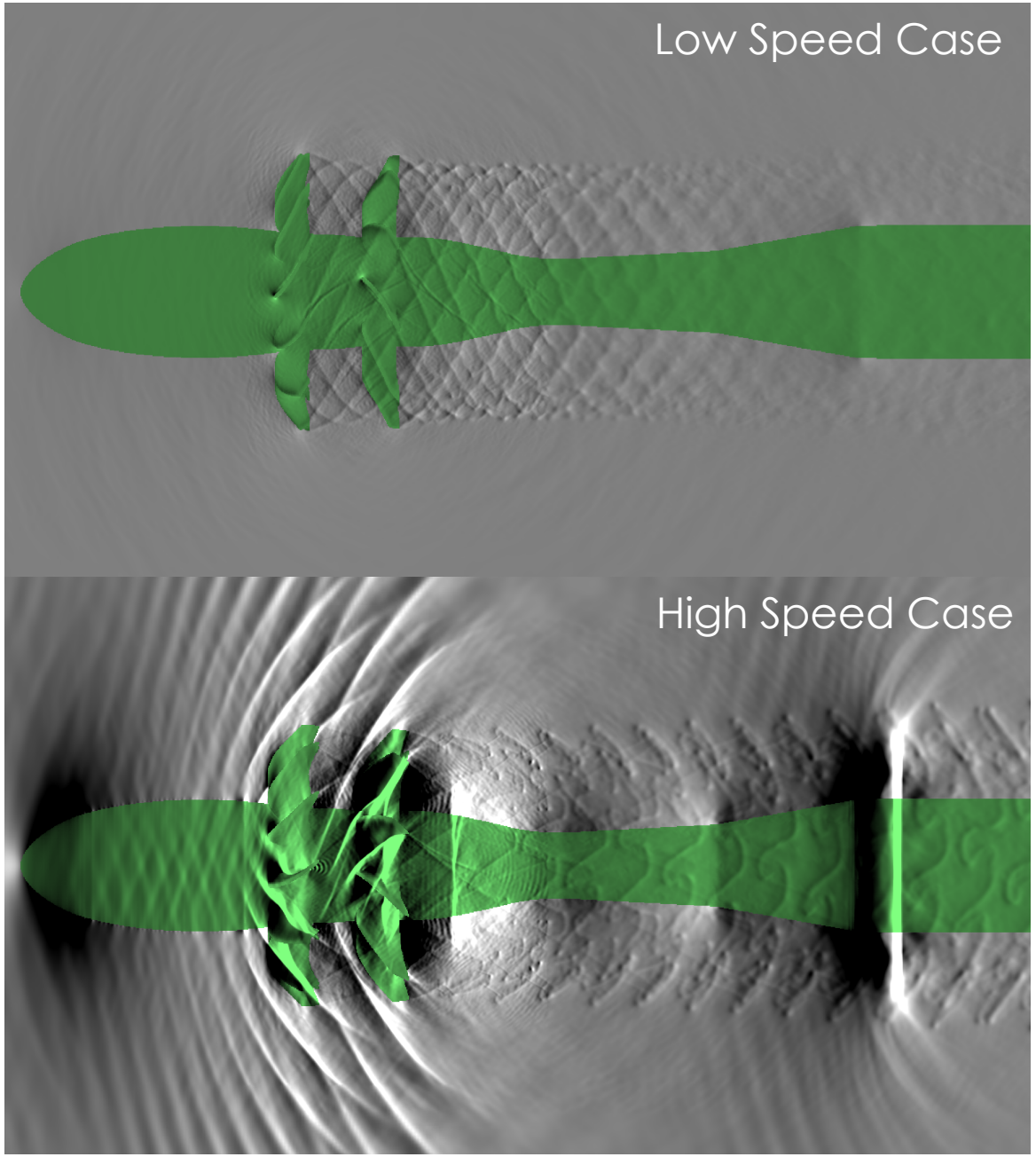

# Odd and Difference Tones

- Following theory by Envia (IJA-2015, Vol 13, No. 3&4)
- Theory predicts dominant tones with SO(m,n)=12m+10n

# Odd and Difference Tones

- Following theory by Envia (IJA-2015, Vol 13, No. 3&4)
- Theory predicts dominant tones with SO(m,n)=12m+10n
- Difference tones decay rapidly? ➔ f(n) and g(n) control the radiation efficiency

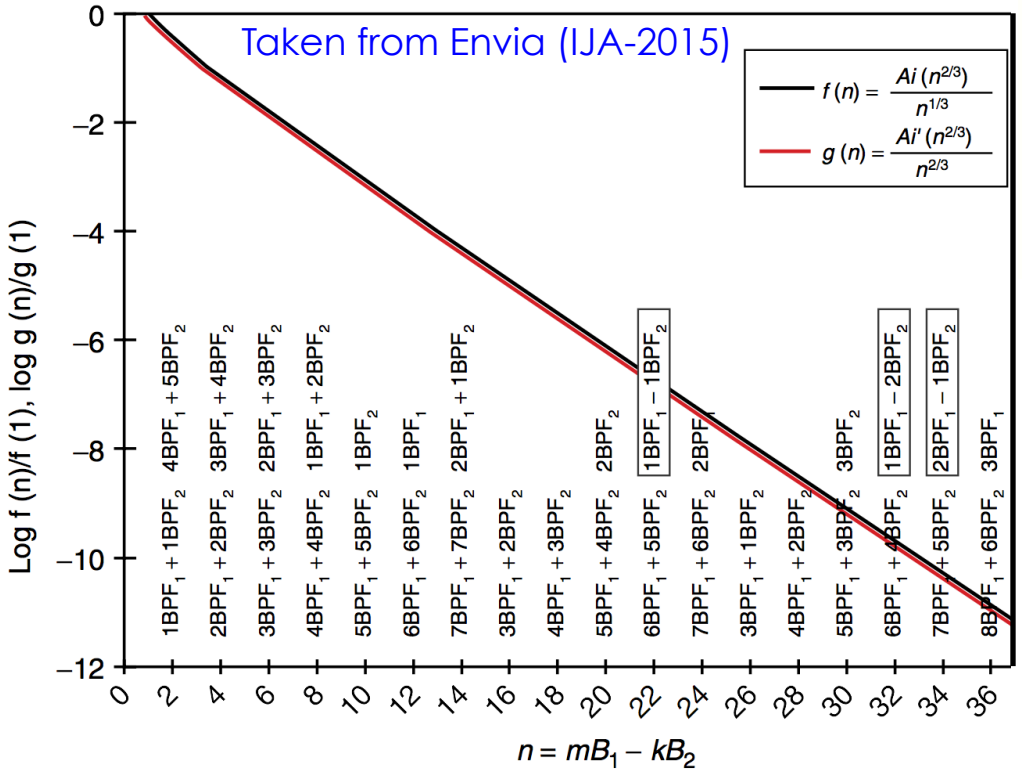


Thickness Noise:

$$p'_{\mathcal{T}_m}(\mathbf{x}) \approx iB_1 \sum_{n=1}^{2} \int_{S_{B_1}} \frac{\mathcal{A}^{(n)}_{\mathcal{T}_m}}{R^n} e^{mB_1(\mu - i\Psi)} \left\{ d_{0,n} \frac{Ai\left[(mB_1)^{2/3}\gamma^2\right]}{(mB_1)^{1/3}} + d_{1,n} \frac{Ai'\left[(mB_1)^{2/3}\gamma^2\right]}{(mB_1)^{2/3}} \right\}_{\mathcal{T}} dS(\tilde{\mathbf{y}}),$$

Loading Noise:

$$p'_{\mathcal{L}_{m,k}}(\mathbf{x}) \approx iB_1 \sum_{n=1}^{2} \int_{S_{B_1}} \frac{\mathcal{A}^{(n)}_{\mathcal{L}_{m,k}}}{R^n} e^{(mB_1 - kB_2)(\mu - i\Psi)}$$

$$\left\{ d_{0,n} \frac{Ai\left[\left|mB_1 - kB_2\right|^{2/3}\gamma^2\right]}{\left|mB_1 - kB_2\right|^{1/3}} + d_{1,n} \frac{Ai'\left[\left|mB_i - kB_2\right|^{2/3}\gamma^2\right]}{\left|mB_1 - kB_2\right|^{2/3}} \right\}_{\mathcal{L}} dS(\tilde{\mathbf{y}}),$$

# Odd and Difference Tones

- Following theory by Envia (IJA-2015, Vol 13, No. 3&4)
- Theory predicts dominant tones with SO(m,n)=12m+10n
- Difference tones decay rapidly? ➔ f(n) and g(n) control the radiation efficiency

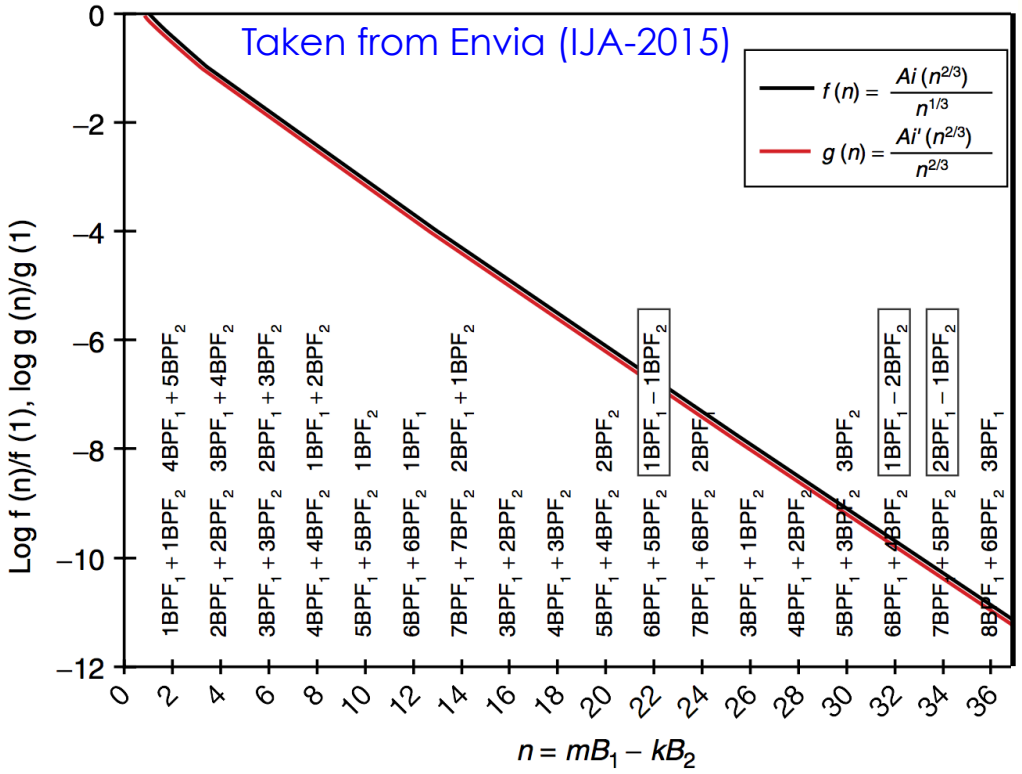


Thickness Noise:

$$p'_{\mathcal{T}_m}(\mathbf{x}) \approx iB_1 \sum_{n=1}^{2} \int_{S_{B_1}} \frac{\mathcal{A}^{(n)}_{\mathcal{T}_m}}{R^n} e^{mB_1(\mu - i\Psi)} \left\{ d_{0,n} \frac{Ai\left[(mB_1)^{2/3}\gamma^2\right]}{(mB_1)^{1/3}} + d_{1,n} \frac{Ai'\left[(mB_1)^{2/3}\gamma^2\right]}{(mB_1)^{2/3}} \right\}_{\mathcal{T}} dS(\tilde{\mathbf{y}}),$$

Loading Noise:

$$p'_{\mathcal{L}_{m,k}}(\mathbf{x}) \approx iB_1 \sum_{n=1}^{2} \int_{S_{B_1}} \frac{\mathcal{A}^{(n)}_{\mathcal{L}_{m,k}}}{R^n} e^{(mB_1 - kB_2)(\mu - i\Psi)}$$

$$\left\{ d_{0,n} \frac{Ai\left[\left|mB_1 - kB_2\right|^{2/3}\gamma^2\right]}{\left|mB_1 - kB_2\right|^{1/3}} + d_{1,n} \frac{Ai'\left[\left|mB_i - kB_2\right|^{2/3}\gamma^2\right]}{\left|mB_1 - kB_2\right|^{2/3}} \right\}_{\mathcal{L}} dS(\tilde{\mathbf{y}}),$$

- Why odd tones? ➔ assumption of blades being identical is not true, thus energy is distributed over all shaft orders causing "extraneous" tones

# Odd and Difference Tones

- Following theory by Envia (IJA-2015, Vol 13, No. 3&4)
- Theory predicts dominant tones with SO(m,n)=12m+10n
- Difference tones decay rapidly? ➔ f(n) and g(n) control the radiation efficiency

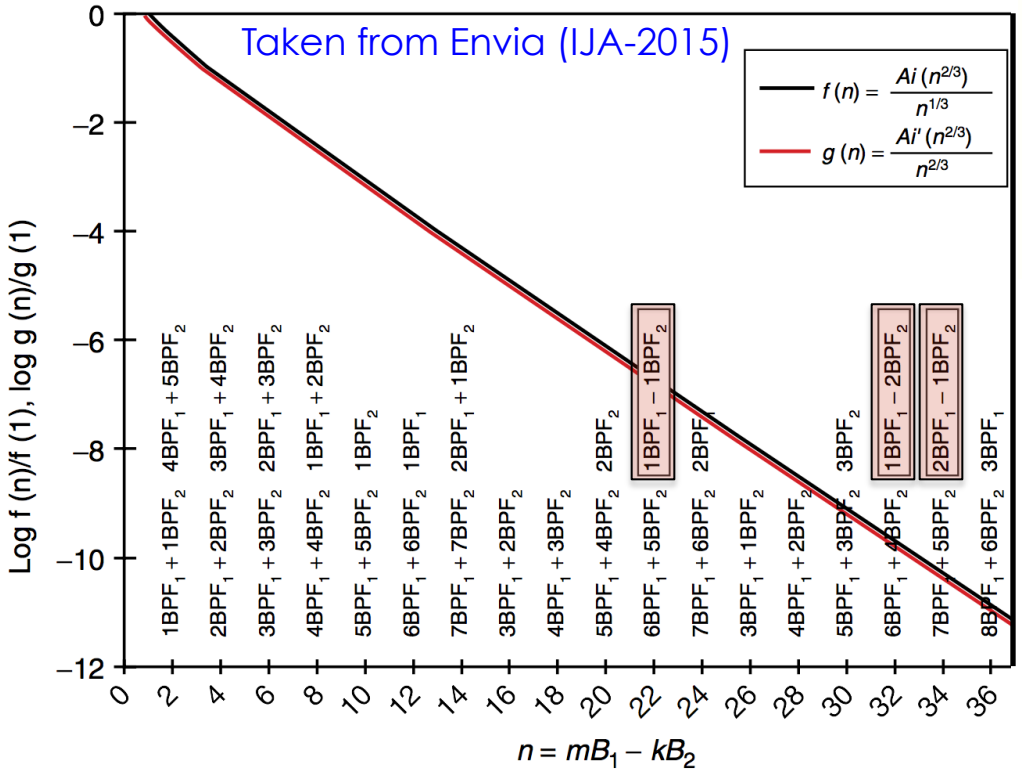


Thickness Noise:

$$p'_{\mathcal{T}_m}(\mathbf{x}) \approx iB_1 \sum_{n=1}^{2} \int_{S_{B_1}} \frac{\mathcal{A}^{(n)}_{\mathcal{T}_m}}{R^n} e^{mB_1(\mu - i\Psi)} \left\{ d_{0,n} \frac{Ai\left[(mB_1)^{2/3}\gamma^2\right]}{(mB_1)^{1/3}} + d_{1,n} \frac{Ai'\left[(mB_1)^{2/3}\gamma^2\right]}{(mB_1)^{2/3}} \right\}_{\mathcal{T}} dS(\tilde{\mathbf{y}}),$$

Loading Noise:

$$p'_{\mathcal{L}_{m,k}}(\mathbf{x}) \approx iB_1 \sum_{n=1}^{2} \int_{S_{B_1}} \frac{\mathcal{A}^{(n)}_{\mathcal{L}_{m,k}}}{R^n} e^{(mB_1 - kB_2)(\mu - i\Psi)}$$

$$\left\{ d_{0,n} \frac{Ai\left[\left|mB_1 - kB_2\right|^{2/3}\gamma^2\right]}{\left|mB_1 - kB_2\right|^{1/3}} + d_{1,n} \frac{Ai'\left[\left|mB_i - kB_2\right|^{2/3}\gamma^2\right]}{\left|mB_1 - kB_2\right|^{2/3}} \right\}_{\mathcal{L}} dS(\tilde{\mathbf{y}}),$$

- Why odd tones? ➔ assumption of blades being identical is not true, thus energy is distributed over all shaft orders causing "extraneous" tones

# Far-Field Spectra

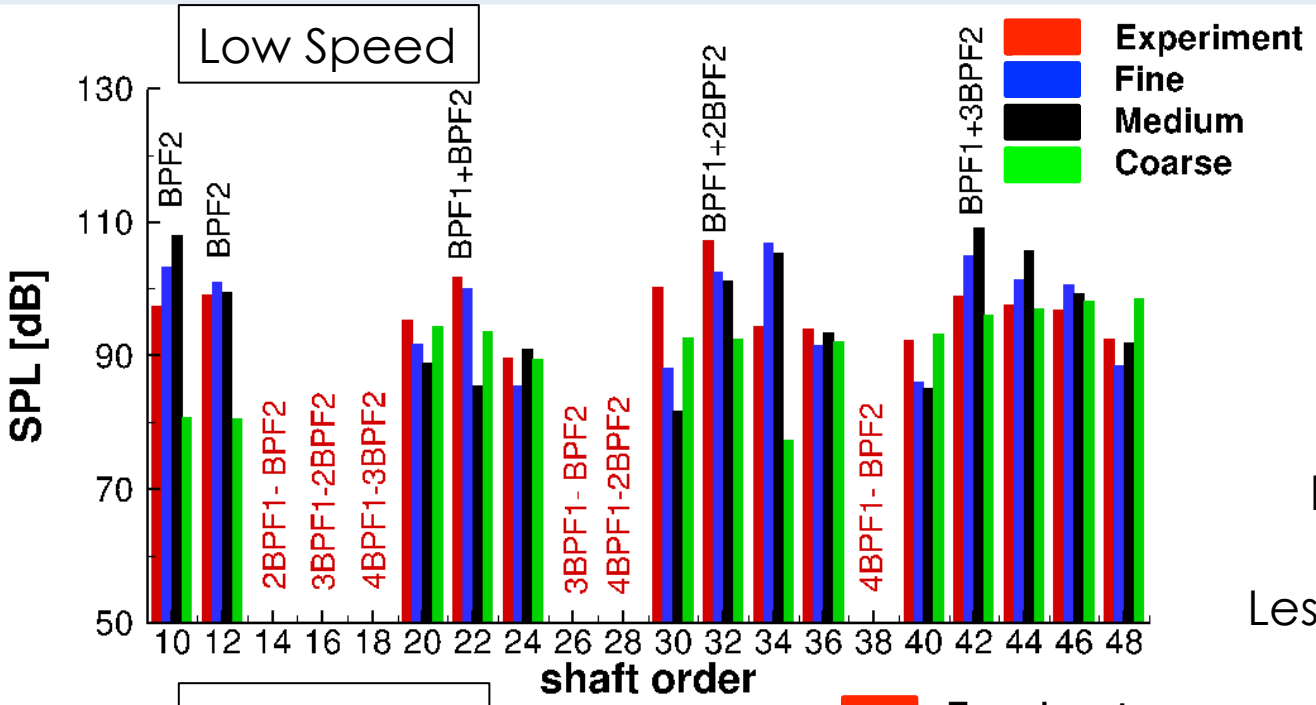


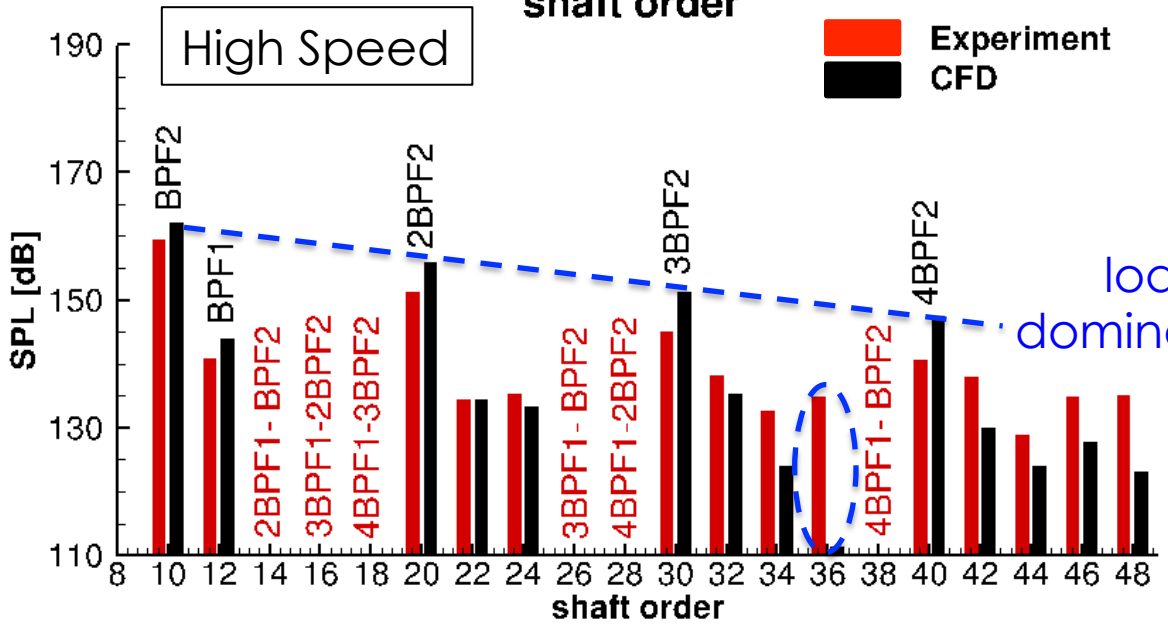


Difference tones excluded:
Less efficient radiators

loading noise is dominant on aft blade

Envia (IJA-2015)

# Spatial Dependence Of Tones (high Speed)

Horizontal Position

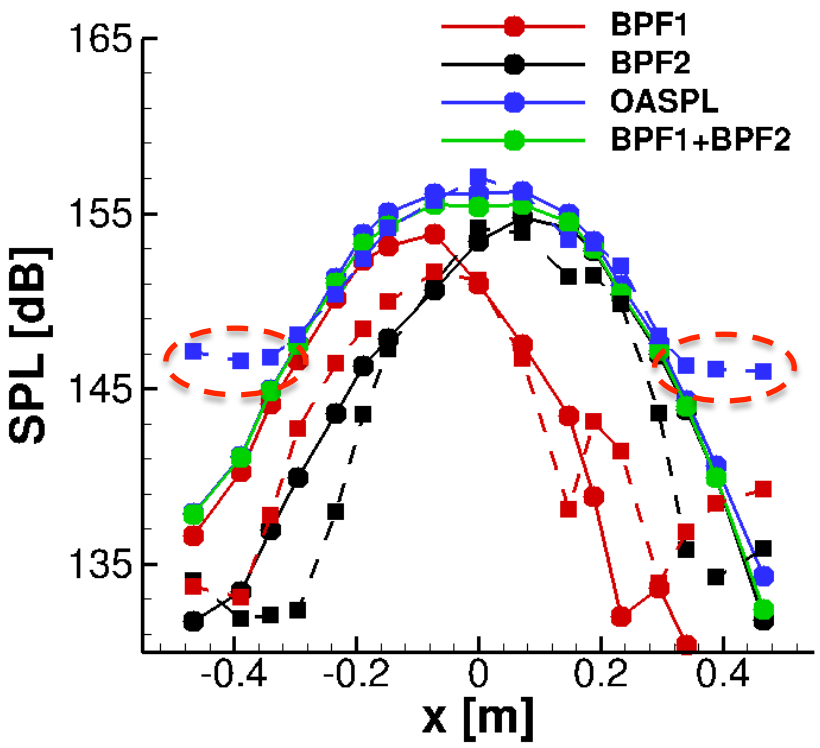


Broadband + Tonal Noise

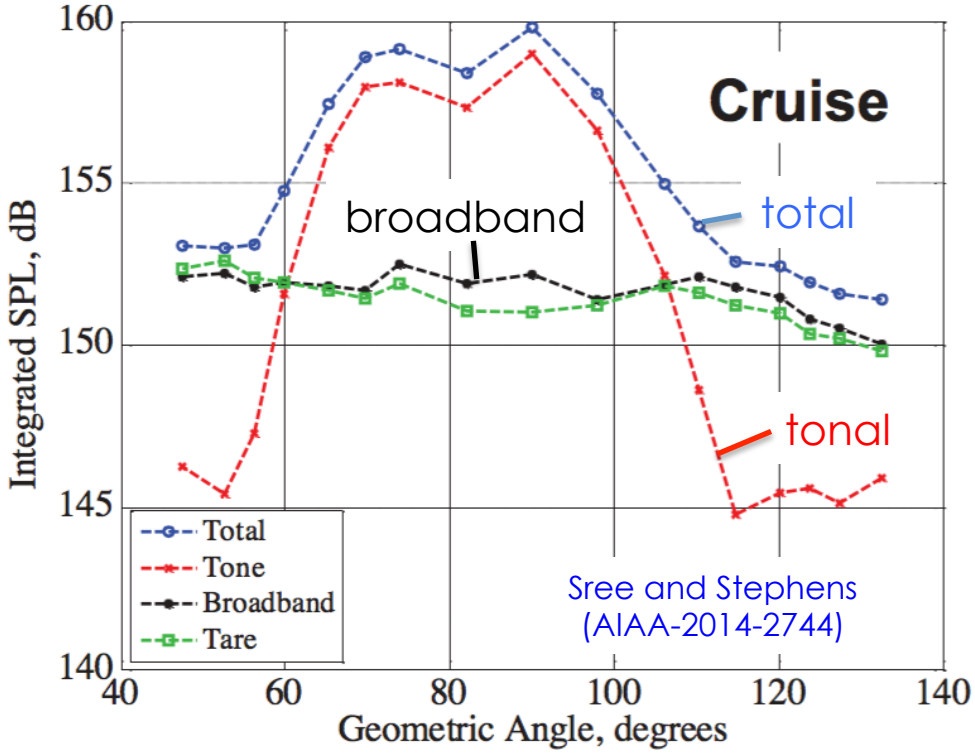


- Fundamental tones dominate OASPL
- Added tonal SPL with BPF1+BPF2 only for comparison
- General trends are well captured for low and high speed cases
- Broadband noise important at small x (<-0.4) and large x (>0.4)

# Near Field Acoustic Analysis (Low Speed)

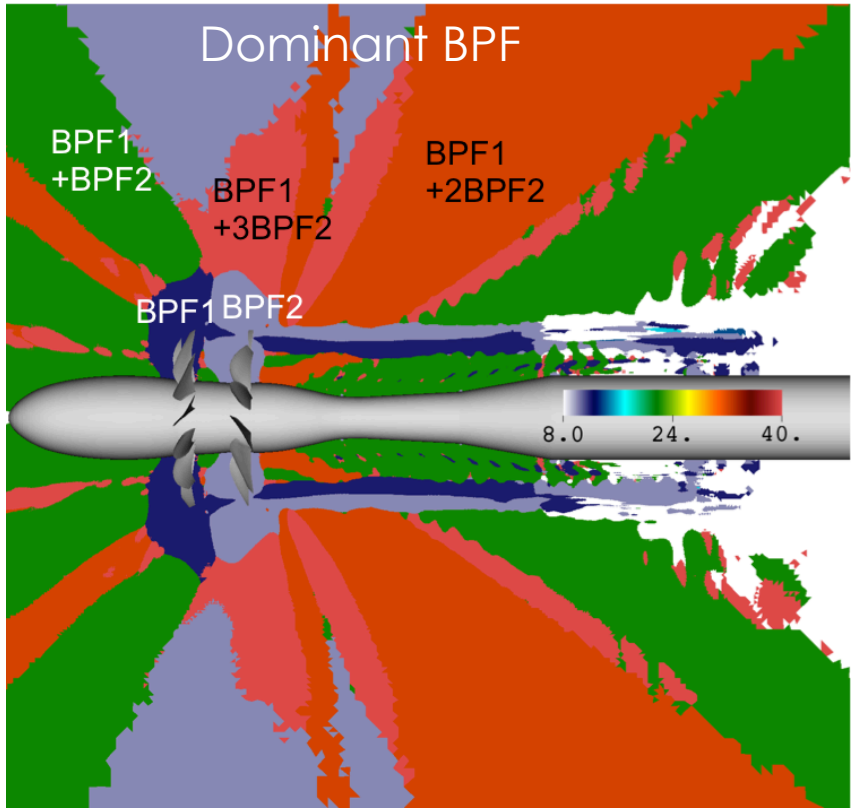


Parameters controlling Radiation Efficiency

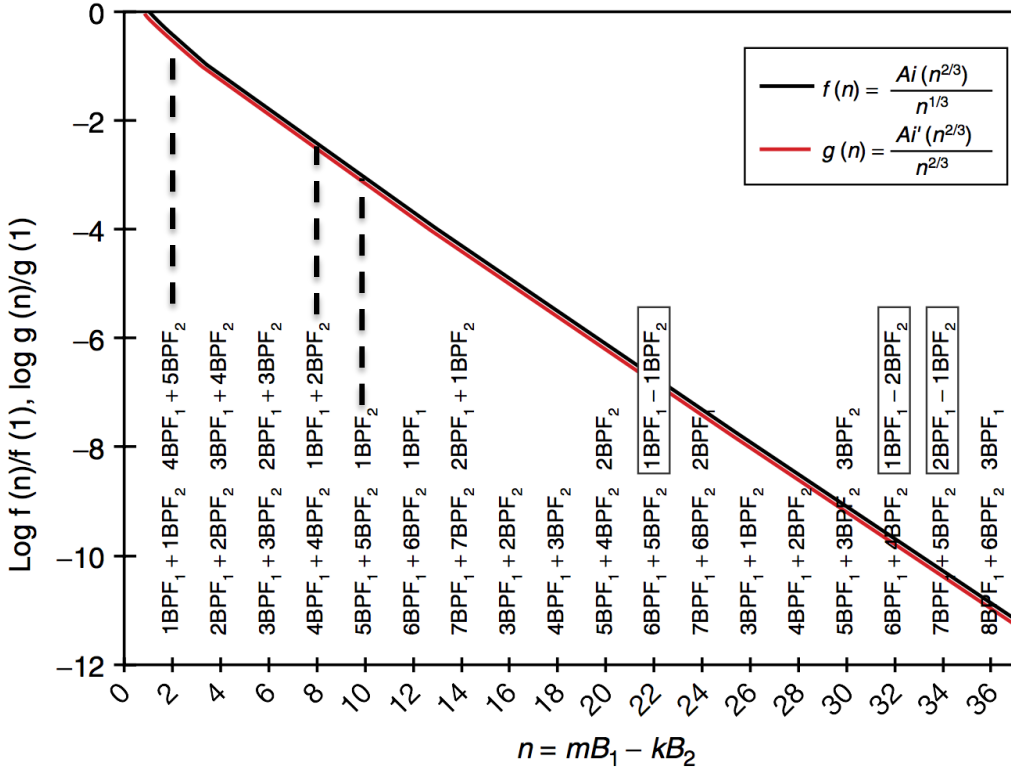


- Analysis captures acoustic waves but also hydrodynamic instability waves
- BPF1 and BPF2 are dominant in a very small region around the rotors and along the tip vortices
- Various higher-order interactions play an important role

# Near Field Acoustic Analysis (BPF1+BPF2)

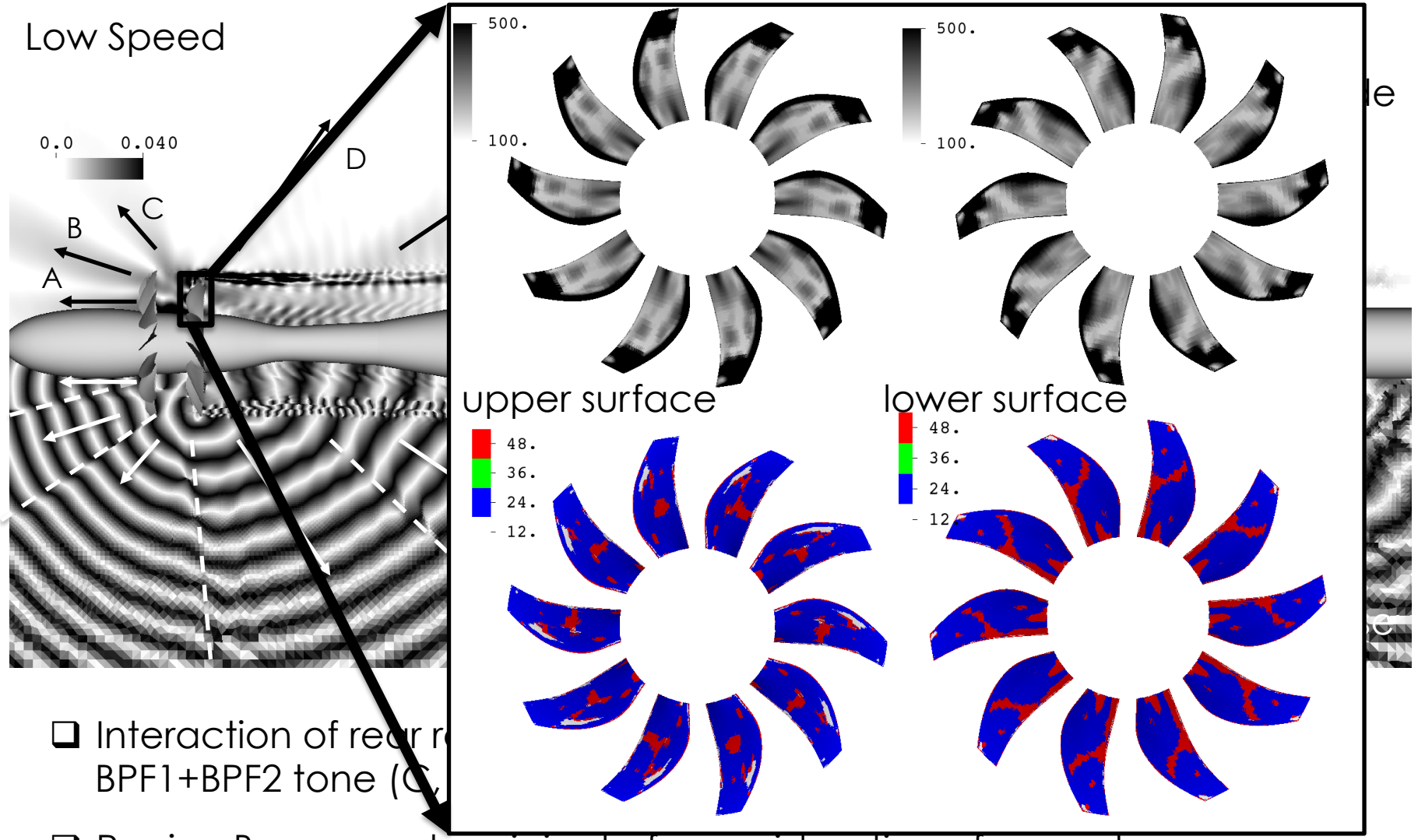


- Interaction of rear r
  BPF1+BPF2 tone (C,
- Region B appears to originate from midsection of rear rotor
- Region E originates from the wake and plays dominant role for large geometric angles